Martin Lampel, BSc

Development of a compact and embedded QEPAS Gas Sensor

Master's Thesis

to achieve the university degree of

Master of Science

Master's degree programme: Information and Computer Engineering

submitted to

Graz University of Technology

Supervisor

Univ.-Prof. Mag.rer.nat. Dr.rer.nat. Alexander Bergmann

Co-Supervisor
Dipl.-Ing. Dr.techn. Philipp Breitegger, BSc

Institute of Electrical Measurement and Sensor Systems

Deutschlandsberg, August 2020

Affidavit

I declare that I have authored this thesis independently, that I have not used other than the declared sources/resources, and that I have explicitly indicated all material which has been quoted either literally or by content from the sources used. The text document uploaded to TUGRAZonline is identical to the present master's thesis.

Date

Signature

Preface

First of all I want to thank my supervisor Alexander Bergmann for the possibility to conduct the master thesis at the Institute of Electrical Measurement and Sensor Systems. It was a very instructive experience to design a sensor and get an insight into the physiscs of the sensor.

Further, I want to thank Philipp Breitegger for the guidance and the help he has provided through the thesis.

I also want to thank Bernhard Schweighofer and Reinhard Klambauer, by supporting me with ideas in the implementation of the firmware and electronic development.

Zusammenfassung

Luftverschmutzung hat erhebliche Auswirkungen auf die Umwelt und die menschliche Gesundheit. Durch diese Tatsachen ist das Interesse an der großflächigen Messung der Luftqualität stark gestiegen. Die räumliche Abdeckung durch herkömmliche Messsysteme ist gering, da die derzeit verfügbaren Sensoren teuer sind oder kostengünstige Sensoren eine geringe Genauigkeit und Langzeitstabilität aufweisen.
Das Ziel dieser Arbeit war die Entwicklung eines embedded und kompakten Sensors für die Messung von NO_2 auf Basis der quartz-enhanced photoacoustic spectroscopy. Diese detektiert Schallwellen mit einer Quarz-Stimmgabel. Die Schallwellen entstehen durch die Absorption eines modulierten Lichts durch den Analyten und der darauf folgenden Druckausdehnung durch die thermische Expansion.

Das entwickelte System besteht aus zwei Leiterplatten. Das Control-and-Sensorboard ist für die Signalerzeugung und Datenerfassung zuständig. Ein Lock-In-Verstärker berechnet aus den erfassten Daten die NO_2-Konzentration. Die zweite Platine, das Mainboard, ist für die Visualisierung und das Speichern der Messdaten zuständig. In der Firmware des Control-and-Sensorboards ist eine Zustandsmaschine für den Messzyklus, ein Lock-In-Verstärker und die Kommunikation über RS485 implementiert. Die Firmware des Mainboards verwendet eine Grafikbibliothek für die Visualisierung und Protokollierung der Messungen auf einer SD-Karte. Als Kommunikationsschnittstellen stellt das Mainboard USB und RS485 zur Verfügung.

Das Sensorsystem wurde in einem Laboraufbau evaluiert und es konnte eine Nachweisgrenze von 27 ppb bei einer Integrationszeit von 58 s dargestellt werden. Diese Ergebnisse machen das Sensorsystem für Luftqualitätsüberwachungsstationen nutzbar, da es ein Überschreiten des Stundenmittelwerts der NO_2-Konzentration laut WHO Richtlinie messen kann.

Abstract

Air pollution has a significant impact on the environment and human health. Through these facts, monitoring of air pollution has gained more interest in recent years. The spatial coverage of monitoring stations is low because the currently available sensor are high-cost or have low accuracy and long-term stability.
The aim of these thesis was to develop an embedded and compact sensor for the measurement of NO 2 based on the quartz-enhanced photoacoustic spectroscopy. Quartz-enhanced photoacoustic spectroscopy detects sound waves with a quartz tuning fork. The sound waves are caused by the absorption of a modulated light by the analyte and the pressure change through the thermal expansion.

The developed system is made up of two circuit boards. The Control-and-Sensorboard is responsible for signal generation and data acquisition. A lock-in amplifier computes from the acquired data the NO_2 concentration. The second circuit board, the Mainboard has the task to visualize and log the measurements. In the firmware of the Control-and-Sensorboard a state machine for the measurement cycle, a lock-in amplifier, and the communication over RS485 are implemented. The firmware of the Mainboard uses a graphic library for the visualization and log the measurements on an SD-card. As communication interfaces, the Mainboard provides USB and RS485.

The sensor system was evaluated in a laboratory setup and a limit of detection of 27 ppb with an integration time of 58 s can be achieved. These results make the sensor system usable for measuring exceedances of the hourly AQ limit value for NO2, according to the WHO.

Contents

1 Introduction

In the recent years air pollution has obtained much attention due to impact on the environment and the human health. Also, the Volkswagen emission scandal where a defeat device was used to activate the emission controls only during laboratory emissions testing, and the emissions of NOx were exceeding the limits in real-world driving. Air pollution is caused by man-made sources such as industry, motor traffic, power plants and natural sources like methane from animals, dust and smoke from wildfire. Air pollution which has been caused by motor traffic is a problem, especially in urban areas owing to the high concentration of vehicles. Air pollutants which are emitted by vehicles are carbon dioxide(CO_2), sulpuhr oxides(SO_2), nitrogen oxides (NO_X) and ozone (O_3). These pollutants are related to health issues such as respiratory diseases or cancer [14]. As a result there is a need to monitor the concentrations of these pollutants. In Europe the limits of concentrations are regulated by the EU directive "on ambient air quality and cleaner air for Europe". In Austria there are currently 94 official air quality monitoring stations(AQM) are operated. By an area of more than 83.000 km^2 and nearly 9 million inhabitants this means there is one station per 100000 inhabitants or one station per 900 km^2 [22]. With this amount of stations the spatial coverage is extremely low. Therefore there is a need to increase the amount of air quality monitoring stations. To do so, it is necessary to apply sufficiently accurate low-cost sensors. The currently available low cost sensors based on electrochemical methods are limited in accuracy and long-term stability.

A well established technique to measure gas concentrations is absorption spectroscopy. The absorption spectrum is primarily determined by the atomic and molecular composition of the gas. By using radiation at wavelengths which matches the gas the radiation is more likely absorped.

One class of absorption spectroscopy is photoacoustic spectroscopy. Photoacoustic spectroscopy uses the photoacoustic effect, which produces a sound wave by absorping radiation and subsequent deactivation. The photoacoustic effect was discovered by Alexander Graham Bell (1880). To acoustically amplify this sound wave an acoustic resonator is used and a microphone to detect the wave. A drawback of these microphone sensors is that they are usually bulky and sensitive to environmental and gas flow noise. Therefore quartz-enhanced photoacoustic spectroscopy (QEPAS) lately attracted the interest of researchers. This method uses a quartz tuning fork (QTF) as resonator and soundtransducer, which offers the advantage of being more immune to environmental noise and a smaller sensor size. However, QEPAS sensors which have been used in the recent research are restricted due to their system design which was restricted to laboratory environments.

The aim of this thesis was to develop an embedded and compact sensor for the measurement of NO_2 based on the quartz-enhanced photoacoustic spectroscopy. The development of such a sensor includes the hardware to control the measurement cycle and measure the analog signal from the QTF. A firmware was developed, which performs the signal processing to obtain the NO_2 concentration. For signal processing a Lock-in amplifier is used, which is capable of accurately measuring a signal in the presence of noise.

2 Background

This chapter gives an overview of the background of NO_2 gas sensors, photoacoustics and lock-in amplifiers. The different sensor principles discussed here, include the chemiluminescence detector, electrochemical sensors and photoacoustic spectroscopy. A lock-in amplifer is used in this thesis. Therefore, the basics of lock-in amplifiers covered in this chapter.

2.1 Overview of commercial gas sensors for NO2

2.1.1 Chemiluminescence Detector

A chemiluminescence detector is based on the emission of light, as a result of the chemical reaction between NO and O_3 [20]. A sketch of the detector is depicted in figure 2.1. The emitted light is proportional to the gas concentration of NO. A photomultiplier or photodiodes are used to measure the emitted light.

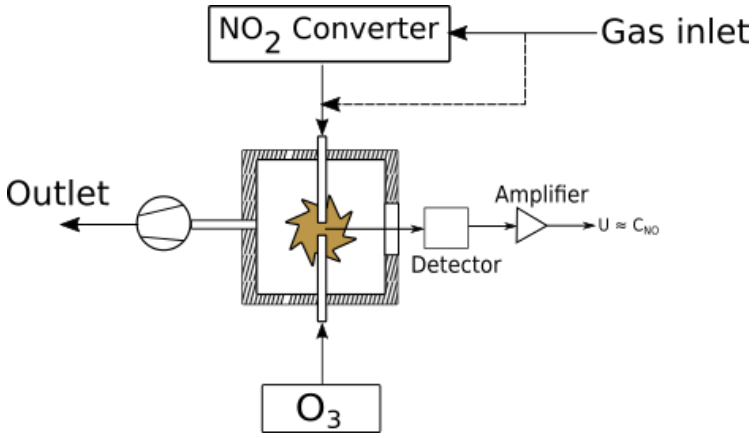

Figure 2.1: Structure of a chemiluminescence detector.

To measure the NO_2 concentration, the following chemical reaction is used in the detector

$$NO + O_3 \rightarrow NO_2 + h\nu + O_2 \tag{2.1}$$

This chemical reaction is based on the reactants NO and O_3. To convert the NO_2 to NO, a catalyser is used. As catalyser are metal or metal oxide used. They are heated up to temperatures exceeding 300 °C.

To produce O_3, an ozonizer can be used. The ozonizer generates O_3 by generating a high electrical field and on the way through the electrical field, O_2 reacts to O_3.

To reproduce measurements, it is required that the temperature, the pressure inside the measuring chamber and the volume flow are constant.

Chemiluminescence based measuring devices are commonly used in environment monitoring stations. E.g, the gas analyzer ECO PHYSICS nCLD 82 S has a minimum detectable limit of 0.12 ppm and a measuring range between 5 ppm and 5000 ppm [17].

2.1.2 Electrochemical sensors

Electrochemical gas sensors are based on the release of electrons, which emerges by a chemical reaction. The resulting current can be used to measure the gas concentration. The chemical reactions use an electrolyte to transfer the charged carriers between the electrodes. The scheme of such an sensor is depicted in fig. 2.2.

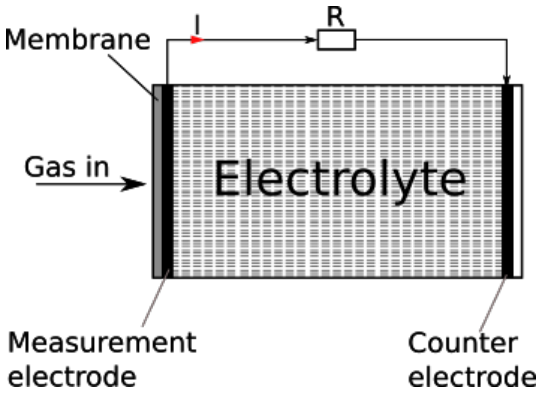

Figure 2.2: Schematic drawing of the electrochemical sensor.

Electrochemical sensors use a liquid electrolyte in a closed casing. The gas gets inside the sensor through a membrane. A chemical reaction on the electrode leads to a release of electrons. The ions move to the counter electrode. At the counter electrode, the electrons recombine with the ions. The electrons flow through an outer circuit, which produces a measurable current. The current is directly proportional to the concentration of NO_2 [20].

One drawback of these types of sensors is their cross-sensitivity to other gases. The reason for this cross-sensitivity is the membrane, which is also permeable for other gas molecules. These other gas molecules contribute to the current.

Moreover, the temperature and pressure have an impact on the current. The diffusion of the molecules through the membrane is temperature-dependent. For high precision measurements, the temperature error must

be compensated. The current is linear dependent on the particle density before the membrane Hence, a pressure increase leads to a higher particle density and the current increases linearly.

The lifetime of these sensors is restricted by chemical reactions in the electrolyte. The lifetime depends on the sensor type and manufacturer. It is usually between one and three years [20].

The sensor principle allows building a sensor with a small footprint and weight, with small energy consumption. This makes the sensors ideal for small devices. The measuring range for such a sensor e.g. alphasense NO2-A43F is 0-20ppm [1].

2.2 Photoacoustic Spectroscopy

The photoacoustic effect was discovered by Alexander Graham Bell during experiments with a photophone in 1880. Photoacoustic spectroscopy (PAS) measures the absorption of electromagnetic waves, light in particular, by the measurement of sound waves. The analyte absorbs the energy from the light, which causes local heating. This local heating generates a thermal expansion, which creates a pressure wave. This sound wave can be detected with a microphone. The principle of PAS is depicted in figure 2.3.

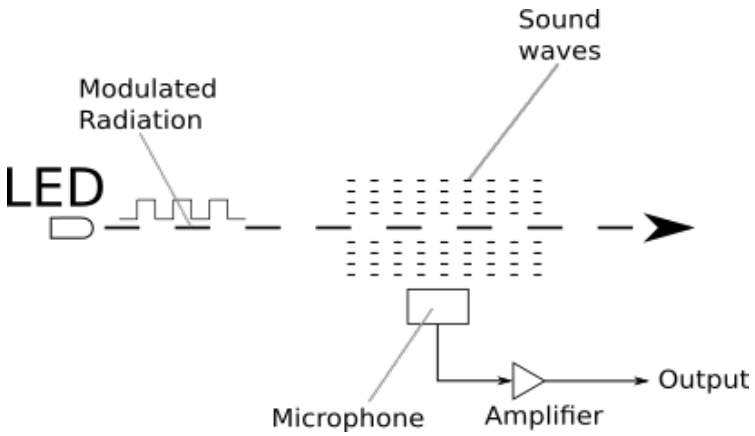

Figure 2.3: Schematic drawing of photoacoustic spectroscope for gas analysis.

The photoacoustic effect starts with the absorption of photons by the analyte molecules. This absorption excites the internal energy states of these molecules. Relaxation processes lead the molecules to return to their initial energy states. These relaxation processes can be divided into radiative processes and non-radiative relaxation processes [3]. A radiative process is the emission of radiation. This process can be neglected if the radiative lifetime is long compared to the time for the collisional deactivation as it is the case for NO2 in the 450 nm region. In the second kind of process, energy is released by collision, which converts the absorbed energy into heat. Since the light source is modulated, the surrounding gas is periodically heated and cooled. These temperature changes generate a sound wave, which can be detected with a microphone.

To measure a gas concentration, the light source is selected with a certain wavelength λ, which is only absorbed by the selected analyte. The photoacoustic signal as a function of the gas concentration is given by Ref. [4]

$$S(c) = P \cdot M(C \cdot \eta \cdot \tilde{\alpha} \cdot c + A_b) \tag{2.2}$$

where P is the power of the light source. M is the sensitivity of the microphone and C is the cell constant.η express the efficiency of the light heat conversion and $\tilde{\alpha}$ is the absorption coefficient of the gas. A_B the efficiency of the background signal generation and c is the gas concentration.

2.2.1 Quartz-enhanced Photoacoustic Spectroscopy

In quartz-enhanced photoacoustic spectroscopy (QEPAS) the same principle is used. However, instead of a microphone a piezoelectric quartz-tuning fork (QTF) with an extremely high Q factor (order of 10000) is used as a sensor for the acoustic wave [11]. Figure 2.4 shows the optical configuration to detect a photoacoustic signal with a QTF. QEPAS has a high immunity to acoustic background noise, which is a very important feature for environmental monitoring. To produce a high signal in QEPAS, it is necessary to modulate the light source at the resonance frequency of the QTF.

The QTF generates piezoelectrical signal, which is amplified with a transimpedance amplifier circuit. The frequency component at the resonance

frequency is then extracted with a lock-in amplifier (see below).

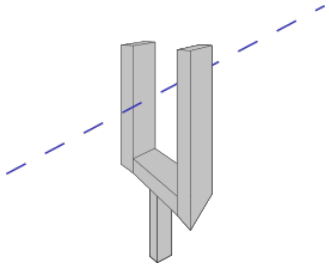

Figure 2.4: Photoacoustic signal detection with a quartz-tuning fork (QTF). The laser beam is perpendicular to the plane of the QTF.

2.3 Lock-in amplifier

Various techniques exist to detect a signal in the presence of high noise. Such techniques are adaptive gilters, matched filters, power spectral density, and the lock-in amplifier. Lock-in amplifiers can be used to extract a sinusoidal signal, which is buried in noise. They can achieve a high signal-to-noise ratio. Lock-in amplifiers are widely used in research and industry [11, 10].

Lock-in amplifiers rely on the orthogonality of sinusoidal functions($\langle x, y \rangle = 0$). Therefore, lock-in amplifiers multiply the input signal with a reference signal. The reference signal specifies the frequency, i.e. which frequency component of the input signal should be detected. Lock-in amplifiers can use two detectors for the in-phase and the quadrature component. The input signal is multiplied with the reference, which is the in-phase component (I). For the quadrature (Q) component the input signal is multiplied with a 90 ° phase shifted reference signal. This is also known as I& Q demodulation. After the multiplication, the signal is filtered by a low-pass to reject noise and the 2ω signal. After demodulation, the signals contain the amplitude and phase information. This can be described through following equations where $x(t) = A\cos(\omega_s t + \varphi)$ is the input and $r(t) = Re^{(-j\omega_r t)}$ is the reference signal

$$
\begin{aligned}
z(t) &= x(t)r(t) && (2.3)\\
&= A\cos(\omega_s t+\varphi)Re^{(-j\omega_r t)} && (2.4)\\
&= A\ R\frac{1}{2}\left(e^{j(\omega_s t+\varphi)}+e^{-j(\omega_s t+\varphi)}\right)e^{(-j\omega_r t)} && (2.5)\\
&= \frac{1}{2}A\ R\left(e^{j((\omega_s-\omega_r)t+\varphi)}+e^{-j((\omega_r+\omega_s)t+\varphi)}\right)\Big|_{\omega_s=\omega_r} && (2.6)\\
&= \frac{1}{2}A\ R\left(e^{j\varphi}+e^{(-j(2\omega_s t+\varphi)}\right) && (2.7)
\end{aligned}
$$

By choosing the cutoff-frequency of the lowpass at $2\omega_s$ one obtains

$$
\begin{aligned}
z(t) &= \frac{1}{2}A\ Re^{j\varphi} && (2.8)\\
z(t) &= \underbrace{\frac{1}{2}AR\cos(\varphi)}_{I=\mathrm{Re}(z(t))}+i\ \underbrace{AR\sin(\varphi)}_{Q=\mathrm{Im}(z(t))} && (2.9)
\end{aligned}
$$

Thus, the magnitude and phase can be directly computed from the demodulated signals

$$
\begin{aligned}
Z &= \sqrt{I^2+Q^2} && (2.10)\\
\varphi &= atan\left(\frac{Q}{I}\right) && (2.11)
\end{aligned}
$$

The integration time constant τ shall be introduced using an analog lock-in amplifier. A RC low-pass can described by follow differential equation

$$
u_{\mathrm{in}}(t) = RC\frac{du_c}{dt}+uc \qquad (2.12)
$$

Solving Eq. (2.12) for u_{c} with the initial condition $u_{\mathrm{c}}(0)=0$ yields

$$
u(t) = \frac{1}{RC}\int_{t-RC}^{t} u_{\mathrm{in}}(s)ds \qquad (2.13)
$$

The integration time can defined as $\tau = RC$. Using the input signal $\sin(\omega_r s + \varphi_r)u_s(s)$ in Eq. (2.14)

$$u(t) = \frac{1}{\tau}\int_{t-\tau}^{t} \sin(\omega_r s + \varphi_r)u_s(s)ds \tag{2.14}$$

For large τ noise and $2\omega_r$ is suppressed and $u(t)$ becomes $\frac{1}{2}A_s\cos(\varphi)$.

The structure of the lock-in amplifier is shown in fig. 2.5. The reference signal is generated by the lock-in amplifier and is applied to the device under test. A lock-in amplifier can be realized as an analog circuit or as a digital implementation. A detailed description of the lock-in amplification can be found in ref. [10].

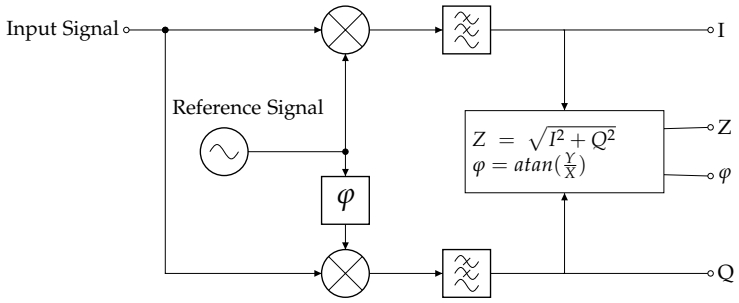

Figure 2.5: Block diagram of a Lock-In Amplifier. The sinusoidal reference signal drives the device and its response is the input signal to the lock-in. The input is multiplied with the reference and 90° phase shifted reference signal. The output of the mixer is filtered by a lowpass to reject noise and 2ω component.

3 Development of the Measurement System

3.1 Concept

In this thesis, a compact device for the measurement of gas concentrations with the quartz-enhanced photoacoustic spectroscopy(QEPAS) technique was developed.

The tasks of this device are to control the measurement cycle and measure certain quantities such as the current, temperature, humidity. With the obtained measurements, signal processing is performed to compute the gas concentrations. The device visualizes and logs the measurements.

This device consists of several circuit boards:

i. Control-and-Sensor Board
ii. Mainboard
iii. Humidity-Temperature-Pressure Board
iv. Quartz-Tuning-Fork Board
v. Thorlabs Laser Driver IP250

The Control-and-Sensor Board is the core component of this device. This board is responsible for the data acquisition, the signal processing and the control of the laser, the valves and pump. The Control-and-Sensor Board generates all required control and modulation signals for the Thorlabs IP250 laser driver. From the Humitiy-Temperature-Pressure (HTP) Board, the Control-and-Sensor Board reads the humidity, temperature, and pressure via an I2C interface.

After a measurement cycle is completed by the Control-and-Sensor board, the data are transmitted via RS 485 to the Mainboard. The Mainboard stores the received data on the SD card and visualizes the data on the TFT display. The USB interface on the Mainboard can be used for configuration purposes and to download the logged data.

The separation of the visualization and measurement tasks into two PCBs has the advantage that the Sensor and Control board can be operated directly with a PC, which is convenient for testing purposes and development of the QEPAS technique in the lab.

The Quartz-Tuning-Fork(QTF) board consists of an amplification circuit for the quartz tuning fork and creates an analog signal which is proportional to the gas concentration. A detailed description can be found elsewhere ref. [6].

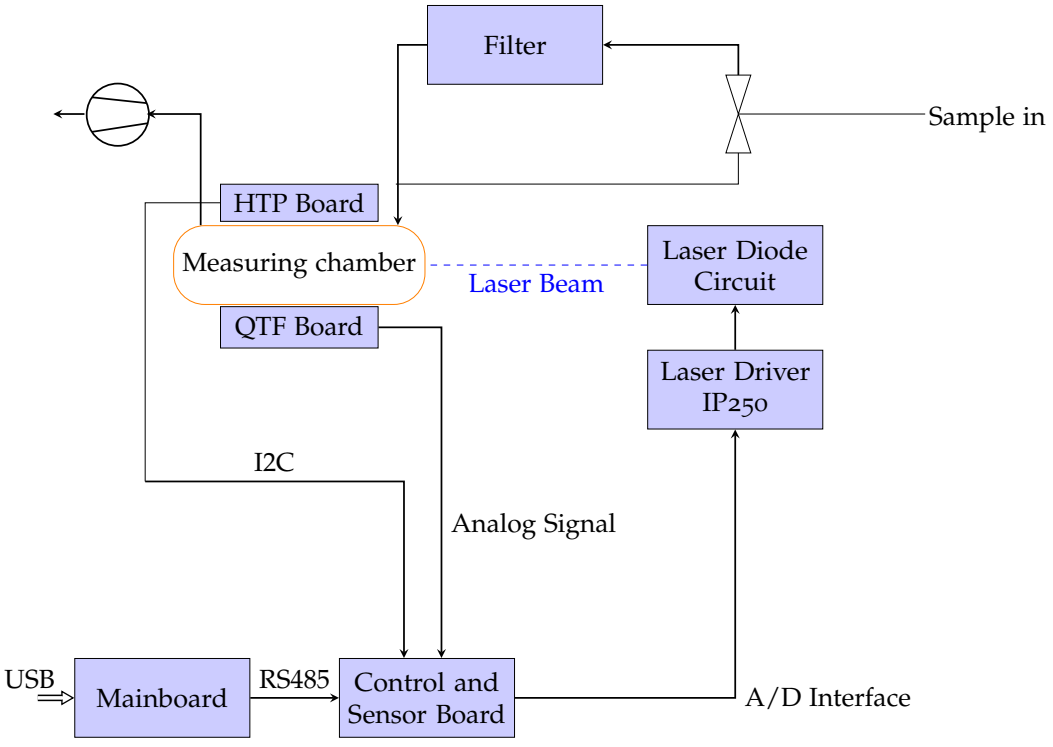

Figure 3.1: Structure of the Measurement System

3.2 Hardware

3.2.1 Control-and-Sensor Board

The measurement of the gas concentrations with QEPAS requires an amplitude modulation of the laser radiation. The laser beam is modulated at the fundamental frequency of the quartz tuning fork(QTF). The laser is focused between the prongs of the QTF. The laser light periodically excites the analyte molecules (here: NO_2), which further heat and cool the surrounding gas, resulting in the production of a sound wave. The sound wave excites vibrations of the QTF, which produces a current, proportional to the analyte concentration[11, 16]. For the detection of the signal from the QTF, a Lock-in amplifier was used.

Therefore the requirements for the circuit are the generation of the modulation signal for the laser driver, and the in-phase and quadrature signals for the Lock-in amplifier. An overview of the Control and Sensor board (CSB) is shown in fig. 3.2. The signals for the Lock-In Amplifier are generated with a DDS IC. The A/D conversion of the QTF, and in-phase, and quadrature signal was done with a $\Delta\Sigma$-ADC. For the communication with the Mainboard, an RS485 interface was used. The valve and the pump are controlled by three transistor stages. The circuits are discussed in more detail in this chapter.

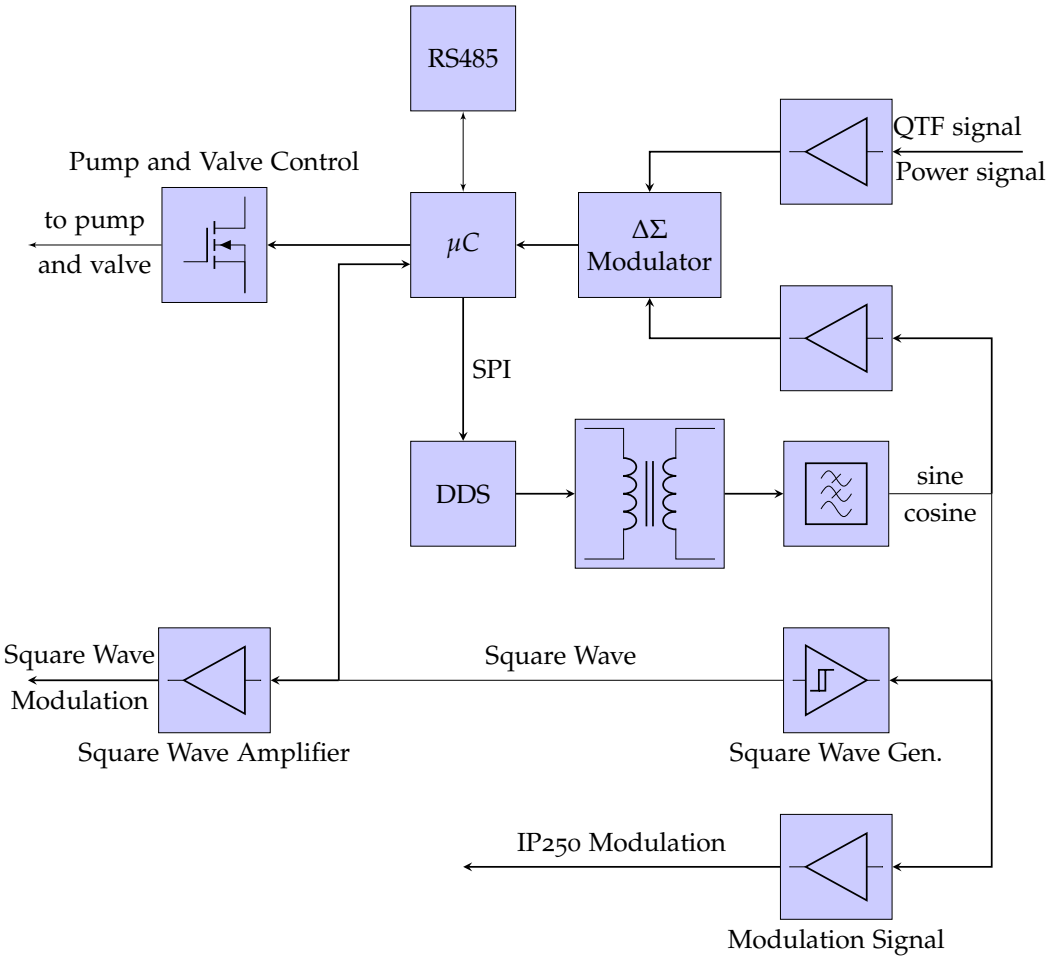

Figure 3.2: Control and Sensor Board block diagram. There are signal generation blocks for the Lock-In Amplifier signals and the Laser modulation signals. A ΔΣ Modulator and Amplifier circuits are used for data acquisition.. For communication purposes, there is an RS485 interface.The Transistor stage block controls the valve and pump.

Microcontroller

As a microcontroller, an STM32F767 was used. This controller features a double-precision floating-point unit and implements DSP instructions. It contains all peripherals which are required in our application.

The clock source for the controller is an 8 MHz oscillator. The PLL of the microcontroller generates the CPU clock of 216MHz from the 8 MHz. The controller is programmed by the SWD interface. For debugging purposes, there are the RX/TX lines from a UART available on a pinhead. An FTDI USB to serial cable can be connected to the pinhead, debug messages are available over a comport.

Signal Generation

To generate the in-phase and quadrature signals for the Lock-in amplifier, a direct digital synthesis (DDS) IC was used. An AD9958 was chosen as DDS IC, which allows a frequency resolution of up to 0.12 Hz. The AD9958 provides two synchronized output channels, where the phase shift for each channel can be configured seperately. The AD9958 is connected to the microcontroller with an SPI interface. The SPI was operated in half-duplex mode in this work. For the clock of the AD9958, a 25 MHz crystal was used.

The output channels are realized through four 10bit current DACs. The current of the DAC can be configured through a resistor. The current is given by the following equation [8]

$$I_{out} = \frac{18.91}{R_{set}} \tag{3.1}$$

To obtain an optimal spurious-free dynamic range (SFDR) performance of the DDS, the current should be limited to 10mA, as suggested in reference [8, p. 18]. The choice for R_{set} was 1.91 kΩ.

To convert these output currents into our in-phase/quadrature signal a center trapped transformer was used (fig. 3.3).

As a reconstruction filter, a 3rd order Butterworth filter was used. The filter is designed as described in ref. [21]. The value for the termination resistor is 50 Ω and the cutoff frequency is 160 kHz. Based on this values the Butterworth filter is designed:

$$L = \frac{R}{2\pi f_c} = 49.73\mu\text{H}$$
$$C = \frac{1}{2\pi f_c R} = 19.89\text{nF}$$

The values for the low-pass filter(n=3) can obtained by

$$C_k = 2\sin\left(\frac{(2k-1)\pi}{2n}\right)C, \quad k = 1,3 \tag{3.2}$$
$$L_k = 2\sin\left(\frac{(2k-1)\pi}{2n}\right)L, \quad k = 2 \tag{3.3}$$

Evalution of Eq. (3.2) yields $C_{72} = C_{76} = C_{79} = C_{80} = 20$ nF and Eq. (3.3) yields $L_2 = L_3 = 100$ µH.

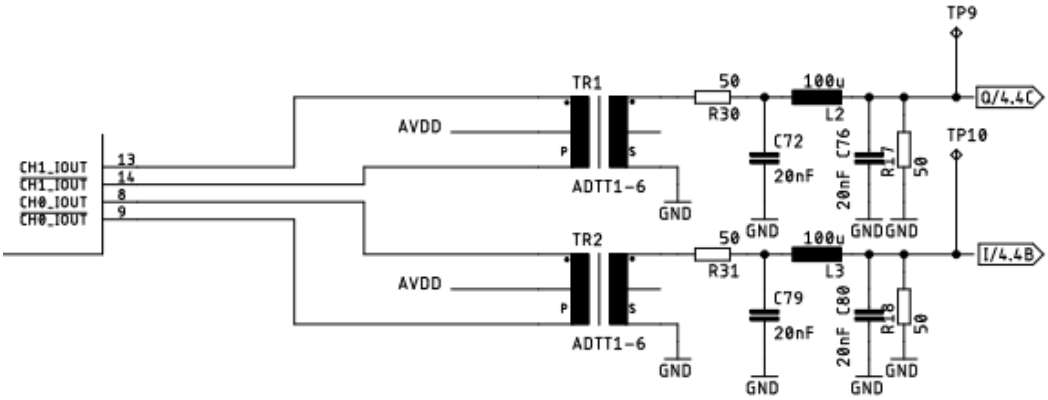

Figure 3.3: The DDS output stage consists of a Transformer and 3rd order reconstruction filter.

Laser Modulation Signals

The analog modulation input of the Thorlabs IP250 Laser Driver allows the user to program the laser injection current in a range from 0 to 250 mA by

applying a 0 to 10 VDC signal, where the transfer function is $1V \triangleq 25$ mA. The analog modulation input can also be used with a sine wave. Since the laser used in this thesis should be operated at 100 mA, a sine wave, with an amplitude of 4 V, is required.

The circuit to generate our modulation signal for the Thorlabs Laser Driver is shown in fig. 3.4. It is a build-up of an inverting amplifier, a clamp circuit, and a differential amplifier. The gain of the inverting amplifier is adjustable with a 10 kΩ potentiometer. The gain is adjustable in range of

$$V_{min} = \frac{R_6}{R_7 + R_{34}} = \frac{12k\Omega}{10k\Omega + 1.2k\Omega} = 1.07$$
$$V_{max} = \frac{R_6 + R_{34}}{R_7} = \frac{12k\Omega + 10k\Omega}{1.2k\Omega} = 18.3$$

which allows the user; to be adjust the Laser current from 6.25 mA to 112.5 mA. The sine wave should always above be 0 V. First, the sine wave is shifted into a negative direction by using a negative clamper(C_1 and D_6). The output voltage after the negative clamper is given with

$$U_{clamp} = U_{C_1} - \hat{u} = -(\hat{u} - U_{F_{D6}}) - \hat{u} = -2\hat{u} + U_{F_{D6}} \tag{3.4}$$

The clamped voltage Eq. (3.4) has a voltage offset of the forward voltage drop of the diode. To remove the offset and generate a positive sine wave, a differential amplifier with unity gain was used. The modulation signal for the Laser Driver is given with

$$U_{mod} = U_{F_{D7}} - U_{clamp} = U_{F_{D6}} - (-2\hat{u} + U_{F_{D6}}) = 2\hat{u} \tag{3.5}$$

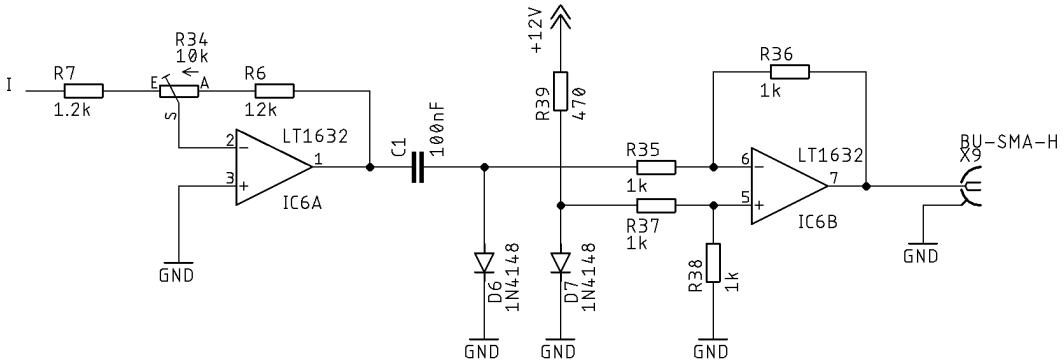

Figure 3.4: Clamping and Amplification Circuit.

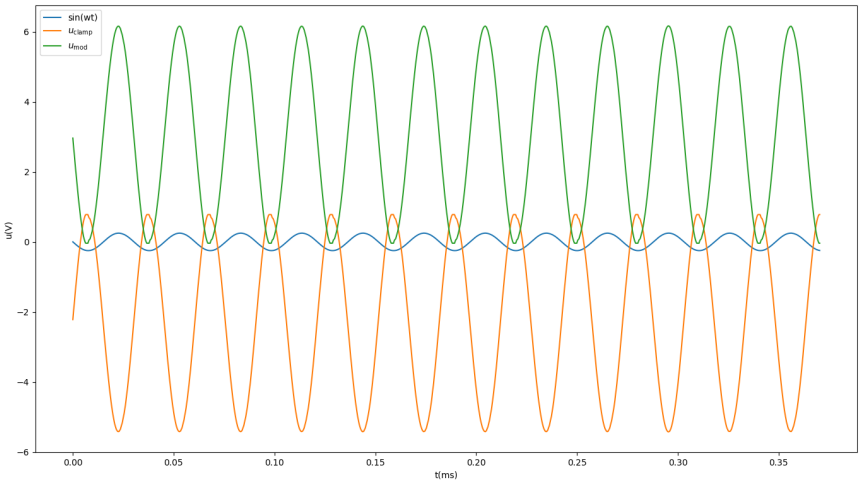

Figure 3.5: Simulation of the Clamping and Amplification Circuit.

For verification purposes, a square wave modulation output (fig. 3.6) exists. This modulation output can be used, e.g. with a Thorlabs ITC4001. The square wave is generated with the dual comparator LT1715. To adjust the amplitude of the square wave, a differential amplifier with a gain of 1.5 was used. The inverting input of the amplifier is connected to a DAC output of

the microcontroller. The output voltage range of the DAC is from 0 to 3.3 V, and the square wave has an amplitude of 5 V. The output voltage of the differential amplifier can be adjusted in the range of 2.5 V to 5 V.

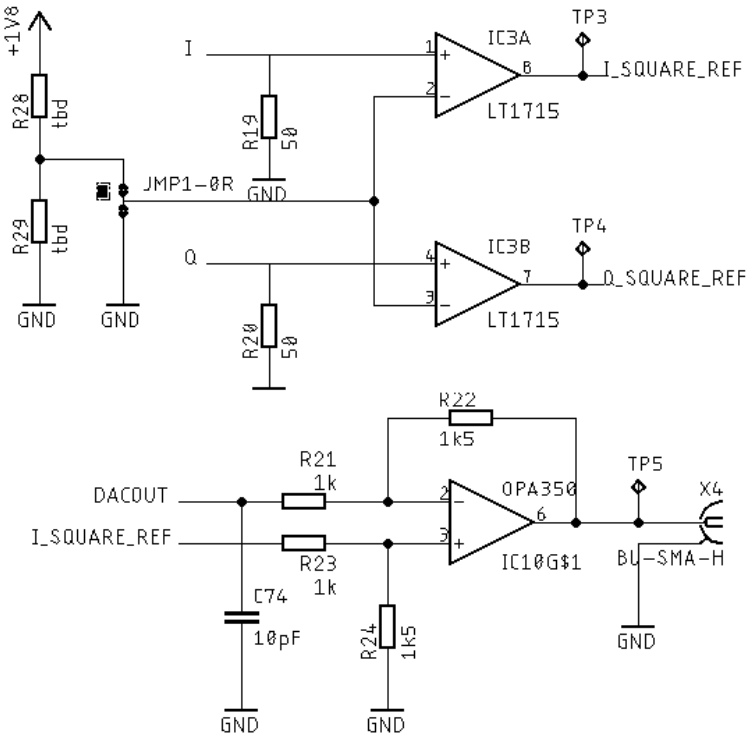

Figure 3.6: The Square Wave Modulation Generation Ciruit generate square signals from the sine/cosine signals with an comparator and amplifies the square wave.

Signal Amplification and Conversion

For the A/D conversion of the signals, a sampling frequency of at least $\approx$ 66 kHz is required. If we assume a sampling frequency of 66 kHz, there is a time slot of 15 µs to transfer the ADC results and do the computations in the microcontroller. Thus an ADC with an SPI interface is used, where the clock runs with 8 Mhz, the transfer of $4 \cdot 20$ bits requires 12 µs. Thus it is obvious, that the transfer between the controller and the ADC is a

bottleneck. A possible solution to address this issue is the usage of an ADC with a parallel interface.

Another solution is to use a ΔΣ ADC. This type of ADCs is composed of a ΔΣ modulator stage and a digital/decimation filter. By using a ΔΣ modulator and implement the digital/decimation filter in the controller/FGPA this bottleneck can be avoided. The implementation of the digital/decimation filter into a controller/FPGA has the advantage that several degrees of freedom exist regarding the properties of the digital/decimation filter.

The STM32F7 family contains a peripheral for this purpose, which is called DFSDM (digital filter for sigma-delta modulators). This peripheral allows configuring the sampling frequency, the resolution, etc. As oversampling frequency of the DFSDM 10.8MHz was chosen. With an oversampling ratio of 64, the sampling frequency is $f_s = \frac{10.8MHz}{64} = 168750$ Hz. The DFSDM filters are configured as fast sinc, which gives a resolution of 19bit. Furthermore, the synchronous sampling of all signals is important. Therefore, the filter stages are configured to run synchronously with the first filter stage.

As a ΔΣ modulator, an ADS1204 was used, which supports four channels. The clock source for the ΔΣ modulator can be selected by an input pin. The clock for the modulator is generated by the DFSDM peripheral of the microcontroller. The CLKSEL pin is tied to the ground to use the external clock source. The bitstreams of the channels are in an SPI protocol format. Each input channel of the ADS1204 is realized as a differential input. A differential amplifier for each input was used to create the differential signals. The input signals to the differential amplifier are the 2.5 V reference from the ΔΣ modulator at positive input and the signal, which should be measured at the negative input.

An anti-aliasing filter with a cutoff frequency of 79 kHz is added after the amplifier.

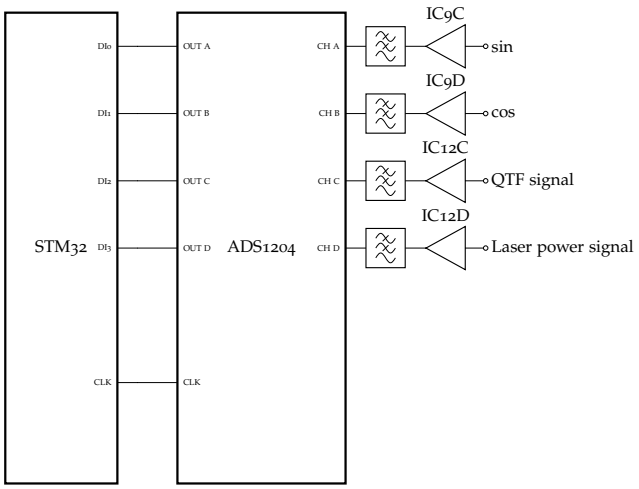

Figure 3.7: ΔΣ Modulator with input stage and Microcontroller connection.

Pump and Valve Stage

The transistor stage consists of a logic level MOS-FET and a flyback diode to prevent voltage spikes. The pump and valve are connected to the PCB with a Phoenix connector. There can be an external voltage supply attached to the connector. On the PCB, there are three transistor stages. These stages are controlled by the microcontroller with a digital pin.

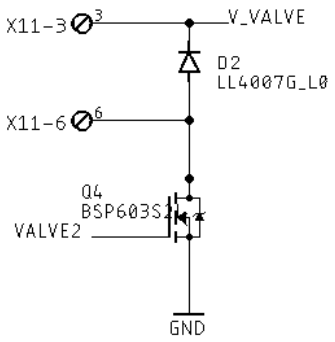

Figure 3.8: Transistor stage to control valve/pump.

Communication

For the communication with the Mainboard, an RS485 bus was used. As a transceiver, a MAX3485 was used. The MAX3485 and the microcontroller were connected over a UART interface. As the control of the direction enable(DE) pin is supported by the UART peripheral, there is no attention required in the firmware for read/write actions. The bus is operated in a half-duplex mode with a transfer rate of 250 kbit/s.

Power Supply

To generate the different supply voltages, LDO's were used. For the analog section, a low noise LDO with a high PSRR would be suitable. An LT3045 was chosen as LDO, which has a PSRR of 85 dB at 30 kHz and the output noise of 2 $\frac{nV}{\sqrt{Hz}}$. The output voltage of the LDO can set by an external resistor. The 5V for the digital and analog section as the 1.8 V for the DDS are generated with this LDO.

For the remaining supply voltages, there are no special requirements. A -5V supply has generated with an LT194ES5. An LF33 generates 3.3 V.

The board must be operated with $\pm 12V$. As polarity protection a MBRS130 schottky diode in plus/minus path was used.

Layout

The layout of the PCB should be designed in such a way that is interference between analog and digital signals is not possible. As suggested in ref. [15] the PCB is separated in a digital and an analog section. The realization of the two sections within the PCB is shown in Fig 3.9.

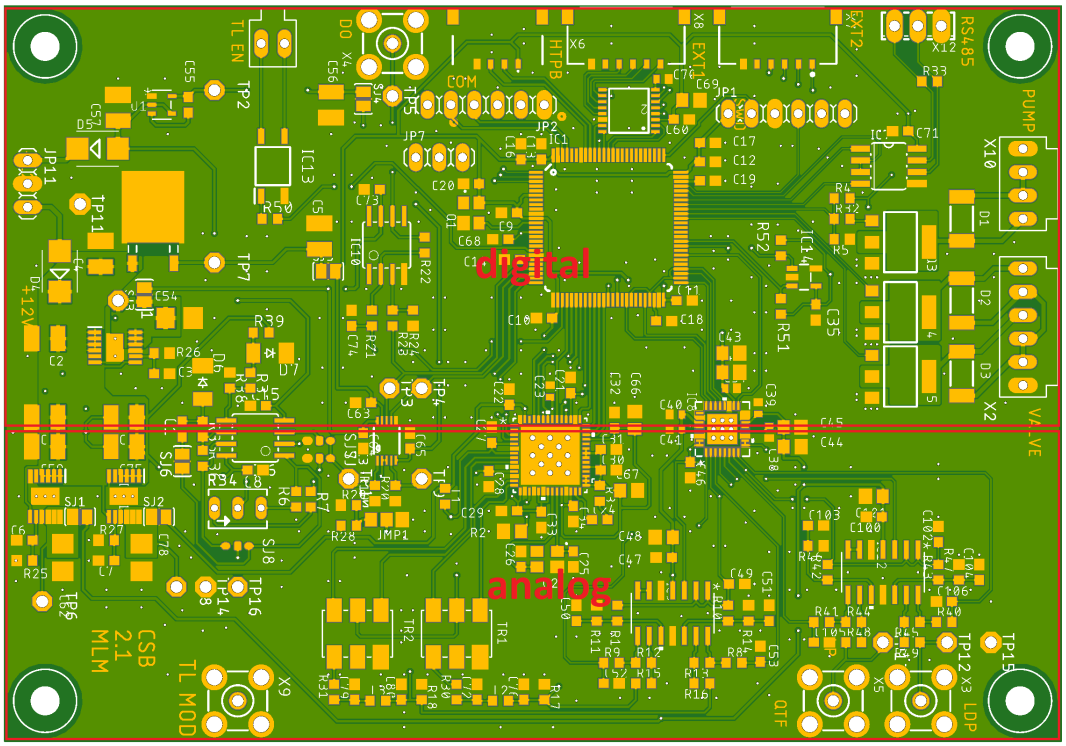

Figure 3.9: Partitioning of the PCB in an analog and digital section.

3.2.2 Mainboard

The mainboard is responsible for the visualization and storage of the measurements. The block diagram is shown in fig. 3.10.

The controller is the same as the Controller-and-Sensorboard, an STM32F767. In this application, the controller is connected to a Display and an SD-card. These connections require many I/O pins. Therefore, a 144 pin LQFP package was chosen.

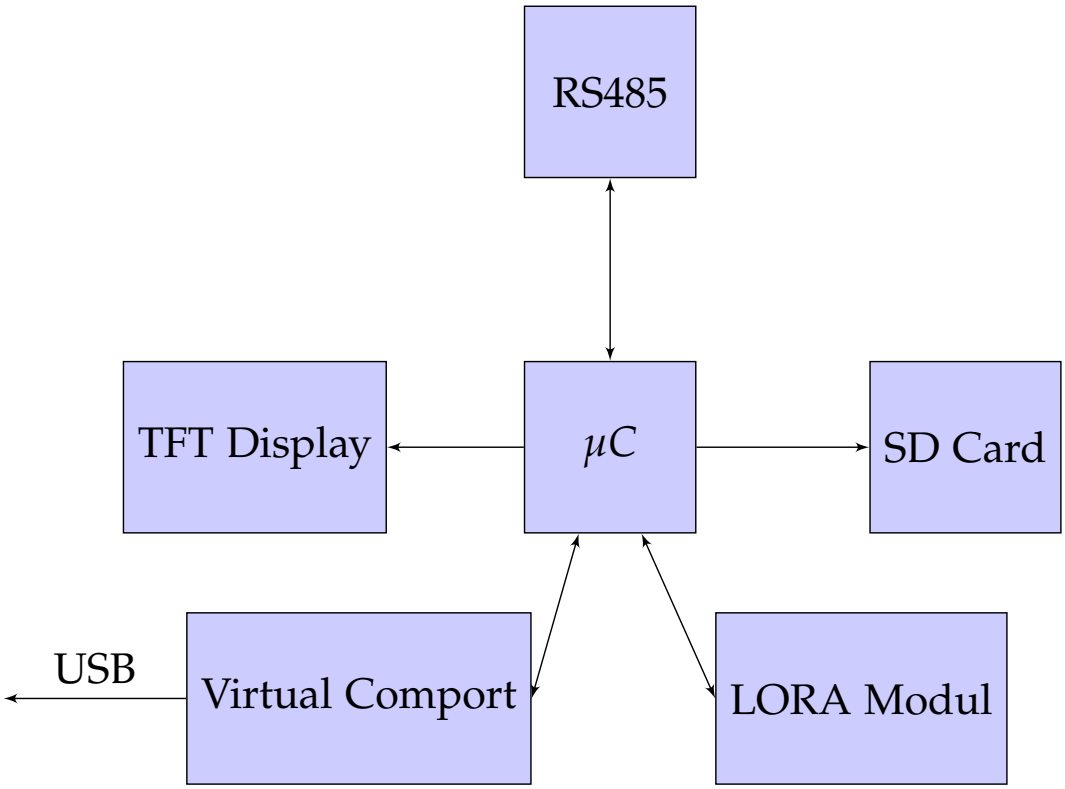

Figure 3.10: The Mainboard has a display for visualization, an RS485, and a USB interface. The SD Card is used to log data.

TFT

For the visualization of the measurements, a TFT display with a resolution of 320x240 was used. The display can be configured in various interface modes. There exist 8bit, 9bit, 16bit and 18bit parallel interface modes. Also, SPI is supported. To reduce the communication overhead the 16bit mode was used (Fig 3.11). To control the display, the Flexible Memory Controller (FMC) peripheral of the microcontroller was utilized.

By using the FMC peripheral, the firmware does not need to take care of the control signals. The FMC handles the display as external memory. There are specific memory addresses used to write instructions or write/read

data. The FMC sets the control signals correctly according to the memory address.

The background light is operated with a Constant Current LED Driver AL5809. This LED Driver provides a current of 50mA.

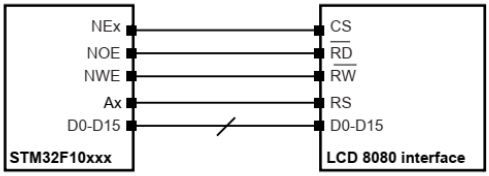

Figure 3.11: Connection FMC to an LCD interface [13]

The touchscreen of the TFT is realized as a resistive touchscreen with a four-wire interface. This kind of touchscreen can be seen as a resistor network(fig. 3.12). To recognize a touch on the screen and reading the position, four pins are required. These pins should be capable of edge detection and interrupt generation and are connected to an ADC of the microcontroller. By configuring the pins according to the scheme in ref. [18, p. 5] and reading the ADC values the position of the touch can be computed.

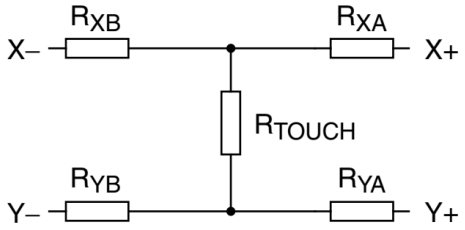

Figure 3.12: four-wire resistive touch screen model [18].

SD Card Interface

The microcontroller has an SDMMC controller, which can be used to connect an SD Card. The SDMMC controller supports different data bus modes. On

the mainboard, the 4bit data bus mode was used. The bus clock frequency is 2.4MHz. To recognize if there is an SD card available, the mounting case consists of a switch(signal CD), which is connected to an I/O pin of the microcontroller.

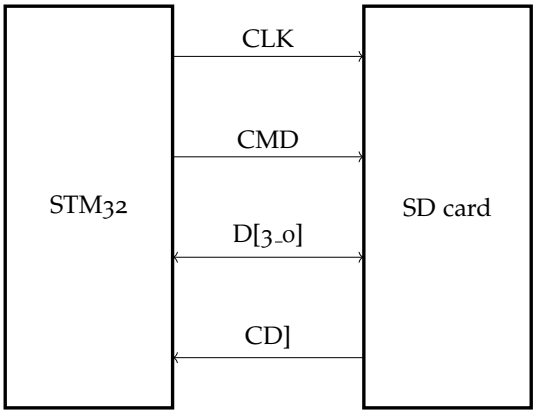

Figure 3.13: SDMMC Interface.

RTC

The measurement data should be logged with a timestamp. This timestamp was created with the real time clock (RTC) of the microcontroller. The RTC is generated with a 32768 Hz crystal. The RTC is powered by a 3V battery if the board is not connected to a power supply. A MOS-FET BS250 switches between the onboard 3.3V supply and the 3V battery voltage. The Battery should only power the RTC. This was done by a Schottky diode in the 3.3V supply path.

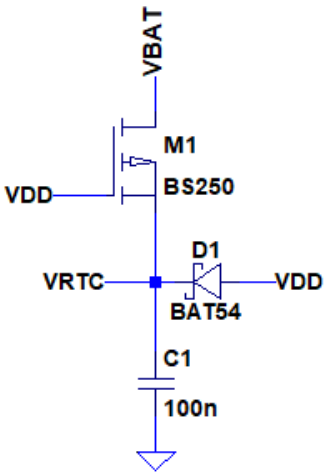

Figure 3.14: RTC voltage circuit.

The circuit was simulated with LTSpice(fig. 3.15). The obtained switching time from the 3.3V supply to the battery is 9.9µs.

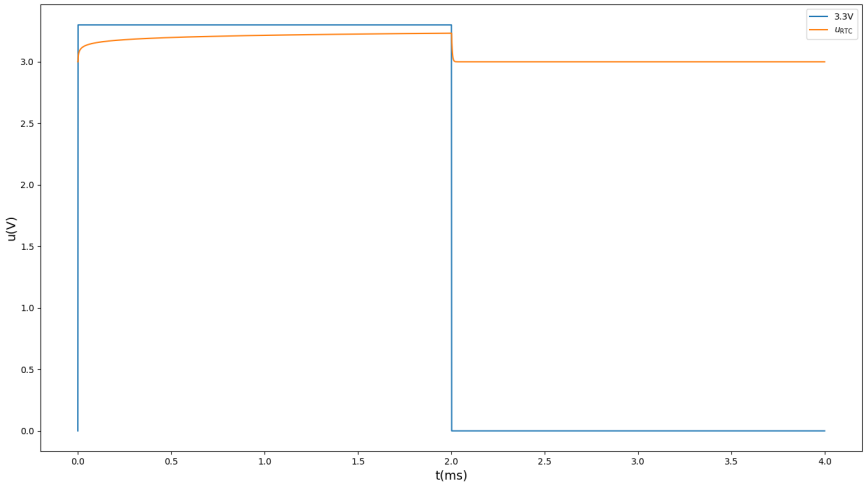

Figure 3.15: Switching Behaviour of RTC voltage circuit.

Communication

For the virtual comport, an FT232BL was used. The connection of the FT232BL to the microcontroller is realized with a UART interface. This interface uses the data and handshake signals for communication. The clock for the FT232BL is generated by a 6MHz crystal. To protect the USB side of the FT232BL against ESD, a USBLC6-2 was used. The circuit is based on ref. [9, p. 2].

The RS485 bus is build up as on the Control-and-Sensor Board. The bus is operated in a half-duplex mode with a transfer rate of 250 kbit/s.

For future extensions, there is the LORAN module CMWX1ZZABZ designated. This module is made up of a LORAN transceiver, a microcontroller with a LORAN stack. The communication to this module is possible over an SPI/I2C/UART interface. The SPI interface was prepared for this purpose on the Mainboard. The transmission line to the antenna is realized in a coplanar wave design. There is also a PI circuit for impedance matching provided. The implementation/test of the LORAN module firmware and hardware are tasks for the future.

3.2.3 Humidity-Temperature-Pressure Board

The purpose of the Humidity-Temperature-Pressure board is to measure the humidity, temperature and pressure in the measurement chamber. These quantities influence the measurement of gas concentration. E.g. the temperature influences the resonance frequency of the QTF.

The HTP Board consists of an MS5803-02BA, which is a pressure sensor. To measure the humidity an SHT31 was used. Both sensors also measure also the temperature. The SHT31 uses an I2C interface, the MS5803-02BA can use I2C or SPI. The board is connected with I2C to the Control-and-Sensor Board. The clock speed of the I2C bus is 400 kHz. The board was powered by the Control-and-Sensor board.

The MS5803-02BA and SHT31 support different I2C addresses. These addresses can be selected by connecting a pin to the ground or VCC. For the

MS5803-02BA the CSB pin is tied to ground the I2C address is 0x77. The I2C address of the SHT31 is 0x44 since the ADDR pin is connected to the ground. The necessary pull-up resistors for SDA/SCL have placed one the HTP board.

3.3 Firmware and Software

3.3.1 Control-and-Sensorboard Firmware

Architecture

In the following section, the firmware of the Control-and-Sensor Board is described. The firmware is built on the top of the Hardware Abstraction Layer (HAL) from STMicroelectronics. The firmware can be grouped in peripheral drivers, the application library, and the application itself. The peripheral drivers are responsible for the interaction with the peripherals such as the SHT31 humidity and the MS5803-02BA pressure sensor. The application library provides utilities that are important for the application. On top of the peripheral driver and the application library the main application is built. The firmware stack is shown in fig. 3.16.

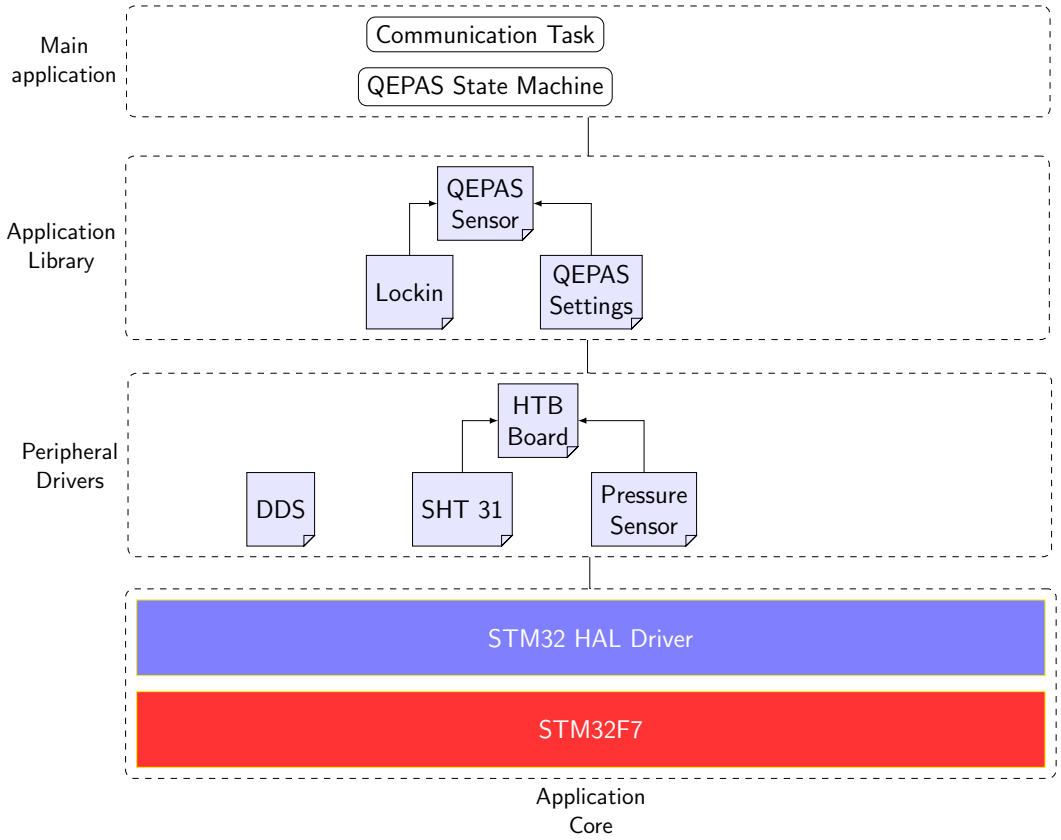

Figure 3.16: Architecture of the CSB Firmware. The firmware can be grouped into Peripheral Drivers, a Application Library and the Main Application.

Peripheral Drivers

The DDS library is used to control the DDS AD9958. The library communicates with the DDS over SPI in a half-duplex mode. It provides functionalities for initialization and reset of the DDS, to adjust the frequency and the phase. In the initialization routine, the PLL of the DDS is configured to generate the internal clock ($\mathbf{f_{DDS}}$ of 500MHz. The DAC outputs are configured in full-scale current mode.

The frequency can be adjusted by a 32bit register and the phase can be adjusted with a 14bit register. With the function dds_set_frequency the out

frequency can be adjusted. The frequency tuning word (FTW) for the 32bit register can be computed by the following equation

$$\mathrm{FTW} = \frac{f_{\mathrm{out}}}{f_{\mathrm{DDS}}} 2^{32} \tag{3.6}$$

The phase can be adjusted with the function dds_set_phase. The function computes the phase offset word (POW) and sets the 14bit register. The POW can be computed in follow manner

$$\mathrm{POW} = \frac{\Phi}{360^{\circ}} 2^{14} \tag{3.7}$$

To adjust the output channel independently, the functions dds_set_frequency and dds_set_phase expect the channel as an argument, which should be adjusted.

The class HTPBoard is an aggregation of the classes PressureSensor and Adafruit_SHT31. The relations between this classes is shown in fig. 3.17.

The PressureSensor class computes the pressure and temperature from the ADC values. The class uses the I2C module from the HAL library for communication. During the construction of the class, a reset of the sensor is performed. After the reset, the calibration parameters are read from the sensor. These calibration parameters are necessary for the computation of the pressure. The pressure sensor contains an ΔΣ-ADC with 24 bit resolution. An ADC conversion is triggered by writing a command byte. This byte contains the information which channel should be converted, the pressure or temperature channel, and the oversampling ratio. In our application, an oversampling ratio of 4096 was used. The method getADCConversion sets the command byte and reads the specified ADC channel from the Sensor. In the method readTempPressure the method getADCConversion is called for both channels and computes the pressure according to the flow chart in Fig. 3.18.

The Adafruit_SHT31 class is based on an Arduino library and is ported to our microcontroller. This class provides methods to read the temperature, humidity and the status of the sensor. Also, a reset method function is

provided. For the port to our microcontroller the methods readTempHum, readStatus, writeCommand are adapted. These functions use the I2C module from the HAL for read/write access.

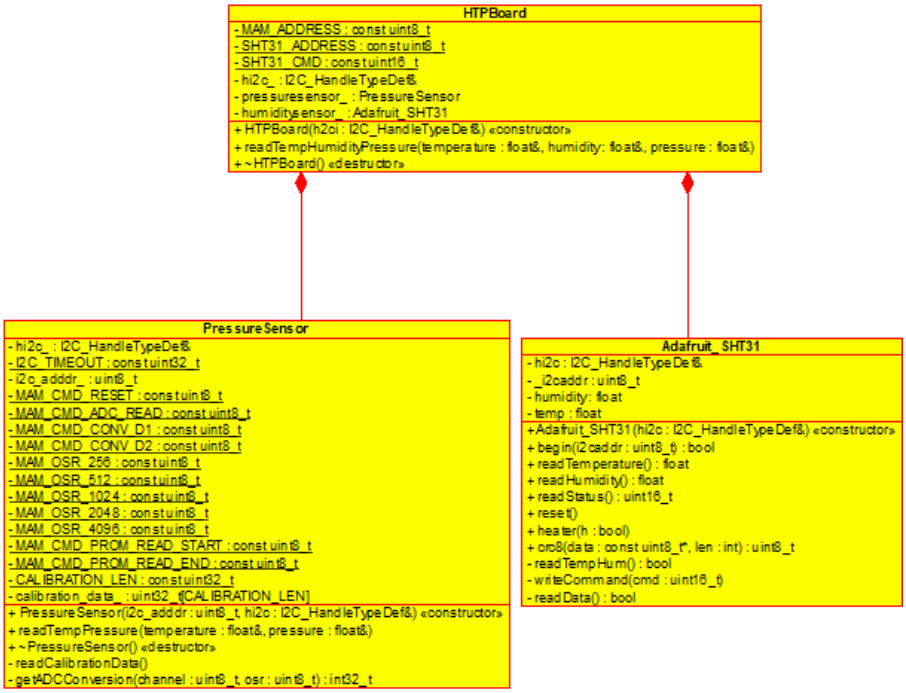

Figure 3.17: Relationship between the entities HTPBoard, PressureSensor and Adafruit_SHT31 .

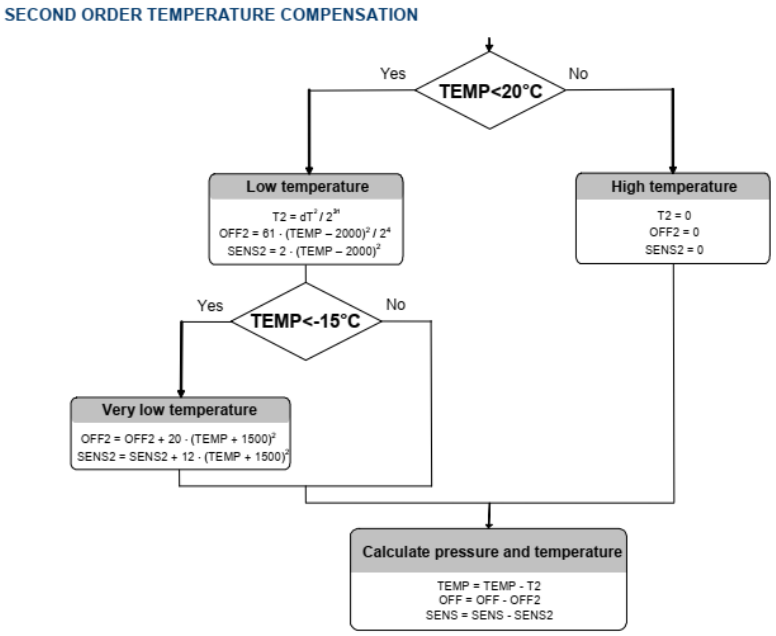

Figure 3.18: Flow chart for pressure and temperature to the optimum accuracy [2].

Application Library

The application library consists of three classes. The Lockin class is an implementation of a lock-In amplifier. The QEPASSettings class contains all settings of the Lock-In amplifier and the measurement cycle. The QEPASSensor class uses the Lock-In Amplifier class and the QEPASSettings class. This class provides methods to control the measurement cycles. The relationships between this classes is shown in fig. 3.19 and will in this section described in detail.

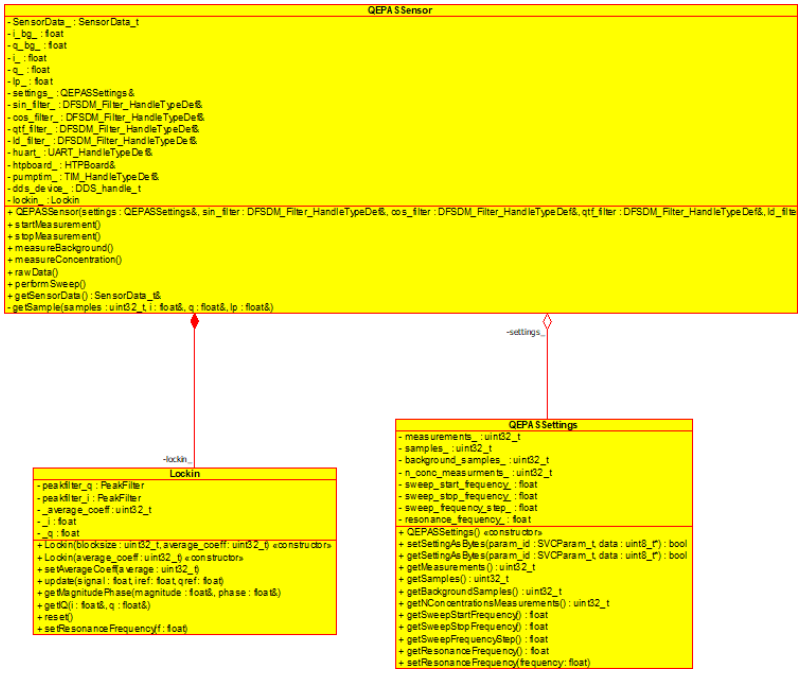

Figure 3.19: Overview of the methods of the classes and their relationships.

As covered in section 2.3, the lock-in amplifier consists of a low-pass. The cutoff frequency should not exceed $2\omega_r$. As low-pass filters, a combination of a moving average and biquad filter are used.

The moving average is given with

$$y[n] = \frac{1}{N} \sum_{k=0}^{N-1} x[n-k], \tag{3.8}$$

which is a finite impulse response (FIR) filter.

The transfer function of the biquad filter is

$$H_{\text{biquad}}(z) = \frac{b_0 + b_1 z^{-1} + b_2 z^{-2}}{a_0 + a_1 z^{-1} + a_2 z^{-2}} \tag{3.9}$$

Biquad filters can be designed as low-pass, high-pass or band-pass filters. In this thesis, the biquad filter was used as low-pass filter. The filter coefficients can be obtained by applying the bilinear transform to analog filter

prototype

$$H_{\text{biquad}}(s) = G\frac{\omega_0^2}{s^2 + \frac{\omega_0}{Q}s + \omega_o^2} \tag{3.10}$$

The filter coefficients are computed with a Matlab script.

Fig. 3.20 shows the frequency response of the mean filter and various cascades of the biquad filter and the mean filter. The taps of the mean filter in Fig. 3.20 are N=168750.

From the comparison of the different frequency responses, it is clear that the moving average filter with his high number of taps dominates in the lower frequencies. At higher frequencies the (cascaded) biquad filters dominate. In the frequency region of interest, which is at $2 \cdot 32768$Hz, the moving average filter achieves an attenuation of -100dB. For the application of the lock-in amplifier in this thesis, the mean filter is sufficient.

The transfer function of the moving average can be computed from Eq. (3.8):

$$\mathcal{Z}\{y[n]\} = \frac{1}{N}\sum_{k=0}^{N-1}\mathcal{Z}\{x[n-k]\} \tag{3.11}$$

$$Y(z) = \frac{1}{N}\sum_{k=0}^{N-1}X(z)z^{-k} \tag{3.12}$$

$$H(z) = \frac{Y(z)}{X(z)} = \frac{1}{N}\sum_{k=0}^{N-1}z^{-k}\Big|_{z=e^{j\omega}} \tag{3.13}$$

$$H(e^{j\omega}) = \frac{1}{N}\sum_{k=0}^{N-1}e^{-j\omega k} \tag{3.14}$$

$$= \frac{1}{N}\frac{1-e^{-j\omega Na}}{1-e^{-j\omega}} \tag{3.15}$$

$$= \frac{1}{N}\frac{(e^{\frac{j\omega N}{2}}-e^{-\frac{j\omega N}{2}})e^{-\frac{j\omega N}{2}}}{(e^{\frac{j\omega}{2}}-e^{-\frac{j\omega}{2}})e^{-\frac{j\omega}{2}}} \tag{3.16}$$

$$= \frac{1}{N}\frac{sin(\frac{\omega N}{2})}{sin(\frac{\omega}{2})}e^{-\frac{j\omega(N-1)}{2}} \tag{3.17}$$

The cutoff frequency of the mean filter is at 0.44Hz. The Bandwidth is 0.88 Hz.

If N is increased in Eq. (3.17), the roll-off increases in the transfer function and the cutoff frequency are reduced. This leads us to the variable average_coeff in the class Lockin. This variable controls the number of filter taps and therefore influences the attenuation and roll-off. By adapting this variable the limit of detection (LOD) can be changed. Furthermore, this variable also controls the time, when new values are available. The default setting for this variable is 168750, which is equal to the sampling frequency. This setting yields a new value for the X and Y signal each second .

Different versions of the LIA have been implemented to find the best one. The first version uses sinusoidal reference signals. The second version uses a Hann window on its input signal to suppress the influence of spectral leakage. The third one uses a square wave as a reference signal instead of a sinusoidal one.

Furthermore, the Goertzel algorithm is compared with the lock-in amplifier. The idea of the Goertzel algorithm is to compute only one complex DFT spectral bin. The algorithm can be used to detect the presence of a sinusoidal signal. More details about the Goertzel algorithm are covered in ref. [12].

The different versions are tested by applying one of the reference signals as an input signal to the lock-in amplifier and the Goertzel algorithm. The magnitude and phase from the different versions are shown in Fig. 3.21.

In the magnitude from the lock-in amplifier with the square wave reference no noise can be observed. The Goertzel algorithm also work well in terms of noise. The lock-in amplifier with the Hann window shows the worst performance. For this application, the phase is also important. The lock-in amplifier versions obtain a stable phase, in contrast to the Goertzel algorithm. Therefore, it is not further considered.

To compare the different LIA versions under real-world conditions, the QEPAS cell was used with synthetic air. For driving the laser diode a Thorlabs LTC4001 was used. The results are shown in Fig. 3.22. With the lock-in amplifier, which uses a sinusoidal reference, the best limit of detection can be achieved. The lock-in amplifier with the square wave reference is worse than the other versions. Since a square wave was used as a reference signal, the harmonics in the input signal have more influence in the lock-in result. In the lock-in amplifier implementation, the version with the sinusoidal references are used.

The method update expects the ADC values for the reference signals as the signal from the QTF as arguments. This QTF signal is multiplied with the reference signals and filtered by the moving average filter. After the N updates are performed, the results from the lock-in amplifier can be read with the methods getIQ or getMagnitudePhase. The reset method sets the lock-in amplifier to its reset values.

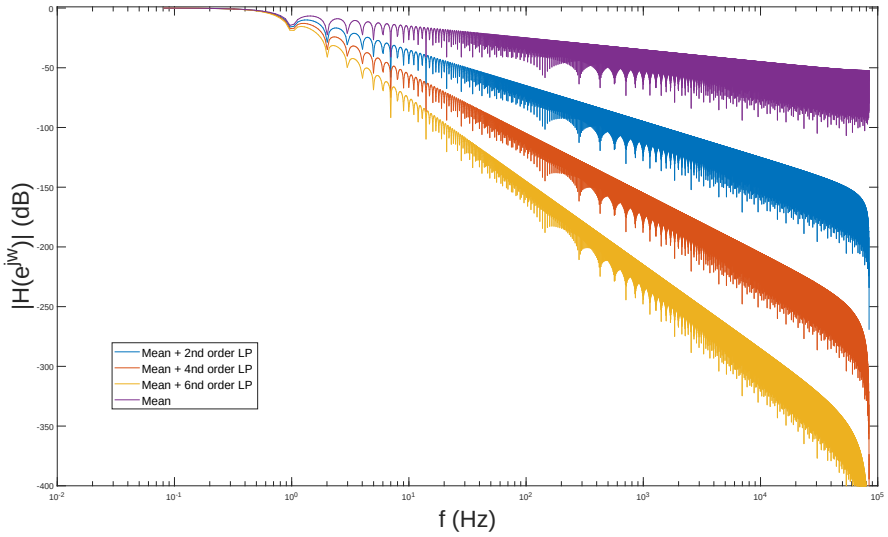

Figure 3.20: Comparision of low-pass filters.

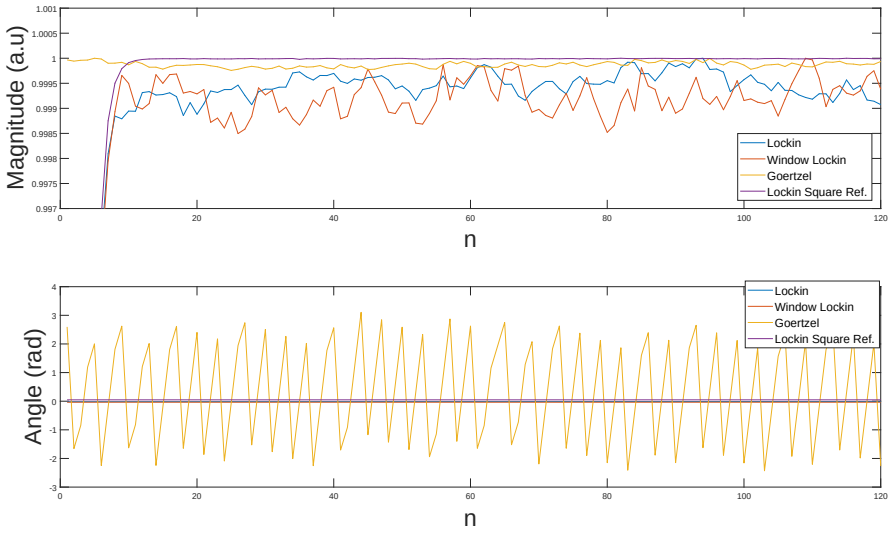

Figure 3.21: Comparision of different Lock-In Implementations.

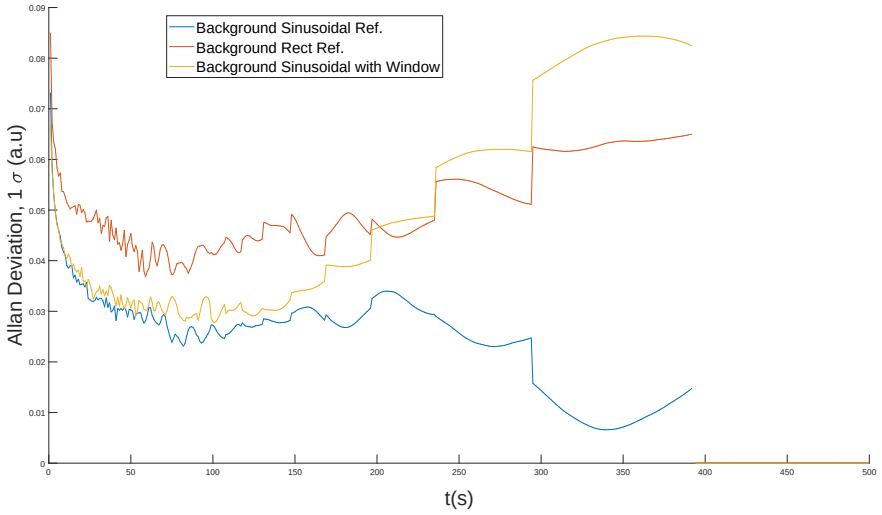

Figure 3.22: Comparision of different reference signals.

The class QEPASSettings stores all settings of the Control-and-Sensor Board. These settings are used for the lock-in amplifier and in the state machine to control the behavior during the measurement cycle.

The following settings can be made:

- Resonance Frequency
  the resonance frequency of the QTF, which is found by a frequency sweep
- Measurements
  This variable is multiplied with Measurement Samples and and is used to set the average coefficient.
- Start Frequency
  The frequency sweep starts at this frequency
- Stop Frequency
  The stop frequency of the frequency sweep
- Frequency Step
  The step size of the frequency during the frequency sweep
- Measurement Samples
  This variable in conjunction with the Measurements variable sets the

average coefficient in the lock-in amplifier. E.g. if Measurements = 168750 and Measurement Samples = 1, the lock-in amplifier yields new values each second. The Measurement Samples are used during the Measurement Concentration State
- Background Samples
  This variable has the same meaning as the Measurement Samples Variable. The difference is, this variable is used in the Background Measurement Step.
- Concentration Measurements
  This variable specifies how many times the Measurement Concentration State is repeated.

The methods setSettingsAsBytes and getSettingsAsBytes convert one setting from its datatype into an array of bytes. These methods are used to convert received settings to its datatype or the settings to its byte representation for transmission.

The QEPASSensor class controls the external and internal peripherals during the measurement and compute the in-phase component, quadrature component and laser power. It utilizes the lock-in and QEPASSettings class. The measurement data is transmitted with the RS485 interface. The format of the measurement data is specified in Fig. 3.23.

There are methods to start and stop the measurement. In the start method the member variables and the lock-in amplifier are set to its default values. Afer setting the default values, the filter units and the laser driver are enabled. The laser and the filter units are disabled by the stop method. In the getSample method the lock-in amplifier runs for the specified integration time, which is specified by the samples arguments. It acquires the number of ADC values and passes these values into the lock-in amplifier. After the integration time is reached, the in-phase, quadrature and laser power are returned.

The methods measureConcentration and measureBackground are very similar. The gas flow through the filter during the background measurement or directly into the measuring chamber during the concentration measurement is controlled by enabling/disable the valve. The method getSample is called with the specified integration time for background or concentration measurement. Also the pressure, humidity and temperature are read from the

HTP-board. After these steps the measurement data is transmitted to the mainboard. The resonance frequency of the QTF can found with a frequency sweep with the method performSweep. For each frequency step, the results are transmitted to the mainboard and the frequency step, which achieves the highest magnitude, is stored as the resonance frequency.

The method rawData stores 25000 ADC samples of each channel and transmit this data over RS485. This method is intended for further processing of the ADC values on a PC.

Communication Protocol

The communication protocol over the RS485 interface is based on a master/slave model. The CSB is the slave. The master can be either the Mainboard or a PC application, which implements the protocol.

The protocol uses four message types (Fig. 3.23). There are command messages, messages to set/read service parameters and a message type of the measurement data. Each message type starts with a function code, which indicates the type of the message. The payload length depends on the message type. An overview of the communication sequences is shown in Fig. 3.24.

The command byte controls the measurement state machine. With the command byte measurements can be started or stopped. There are commands to start a frequency sweep or recording the raw ADC values. The acknowledge on a command message indicates a success if the command executed or an error.

The Set Service Parameter function code can be used to set the parameters, which are described earlier (3.3.1). This message type has as payload the parameter id and the data of the parameter. The order of the bytes is in little-endian. The response of the slave device is a status. If the parameter id is known and the parameter successfully set, the status is one else zero.

To read a parameter, the Read Service Parameter function code can be used. The payload of this message is the parameter id. The slave device responds with status one if the parameter successfully read or zero. However, the

slave device always responds with 5 bytes. The data bytes are only valid if the status is one.

The measurement data message does not work according to a master/slave model and is only sent by the slave device. This message is sent during a frequency sweep or when the device is in the measurement state. The measurement data type is shown in Listening 3.1. The mode indicates if the measurement is recorded during a frequency sweep or a measurement. The frequency is the current resonance frequency of the variable. In each measurement data are the current in-phase and quadrature component and the in-phase and quadrature component from the background are included to compute the concentration.

```
typedef struct __attribute__((packed))
{
        uint8_t mode;
        float frequency;
        float I;
        float Q;
        float IBG;
        float QBG;
        float T;
        float P;
        float H;
} SensorData_t;
```

Listing 3.1: Measurement Data

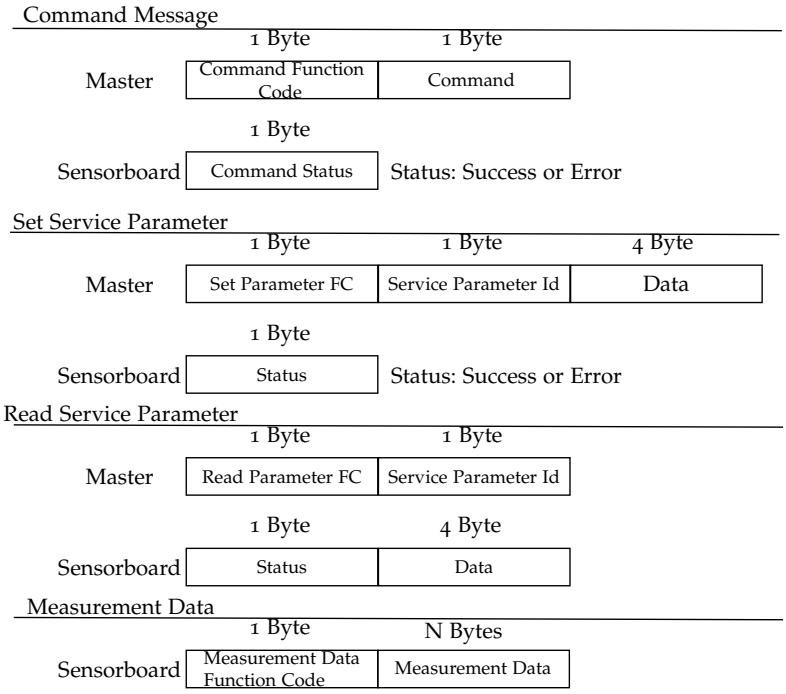

Figure 3.23: Communication Protocol Messages.

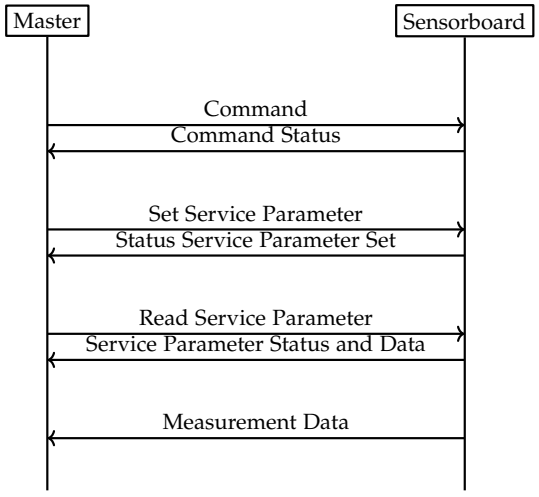

Figure 3.24: Communication Sequences.

The processing of messages on the CSB is interrupt controlled. In the interrupt service routine, each received byte is stored in an array. The length of each message is known by the function code. If all bytes have been received, a flag is set. The function communication_task polls for this flag. The function processes the received message if the flag is set and takes action depending on the function code.

QEPAS state machine

A state machine was implemented to control the measurement cycle. The state machine is shown in Fig. 3.25. The state machine uses the methods of the QEPASSensor class. The transition into states Data Record, Raw Data Record, Frequency Sweep, Start and Stop measurement can only be triggered by a command message.

The measurement cycle starts with the start command message and continues until the stop command message is received. After the start state, the state machine executes the frequency sweep state which determines the resonance frequency by a maximum search. When the frequency sweep is finished, the state machine continues with the background measurement at the determined resonance frequency. The background measurement is necessary since the scattered radiation absorbed inside the gas cell produces a sound at the TF resonant frequency, thus generating a coherent background [16].

The next state is the concentration measurement. The in-phase and quadrature component of the signal is measured. The state machine stays in this state until two conditions are fulfilled. The first condition is the number of concentrations measurements. If this number reached, the state machine switches into the background measurement state. The second condition is to ensure that all measurements are done at the resonance frequency of the QTF. The resonance frequency can be shifted by a temperature change in the cell or change over time. Therefore, if the temperature changes larger than 2° C or 30 minutes passed since the last frequency sweep, the state machine goes into the frequency sweep state.

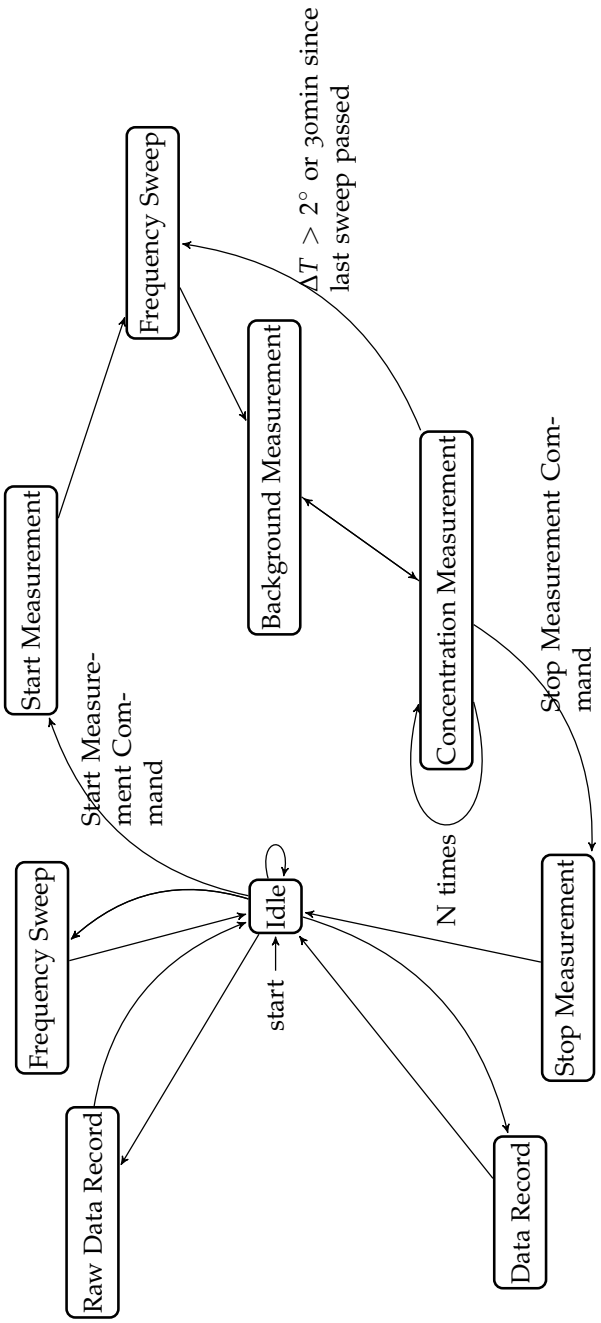

Figure 3.25: QEPAS State Machine.

3.3.2 Mainboard Firmware

The tasks of the Mainboard firmware are the visualization and logging of the measurements. For the visualization the open source embedded graphics library LittlevGL was used. The measurements are logged on the the SD-card. As filesystem for the SD-card FATFs was used. On top of the HAL and these libraries, there are classes that provide the functionalities for the visualization and logging. The firmware is shown in Fig. 3.10.

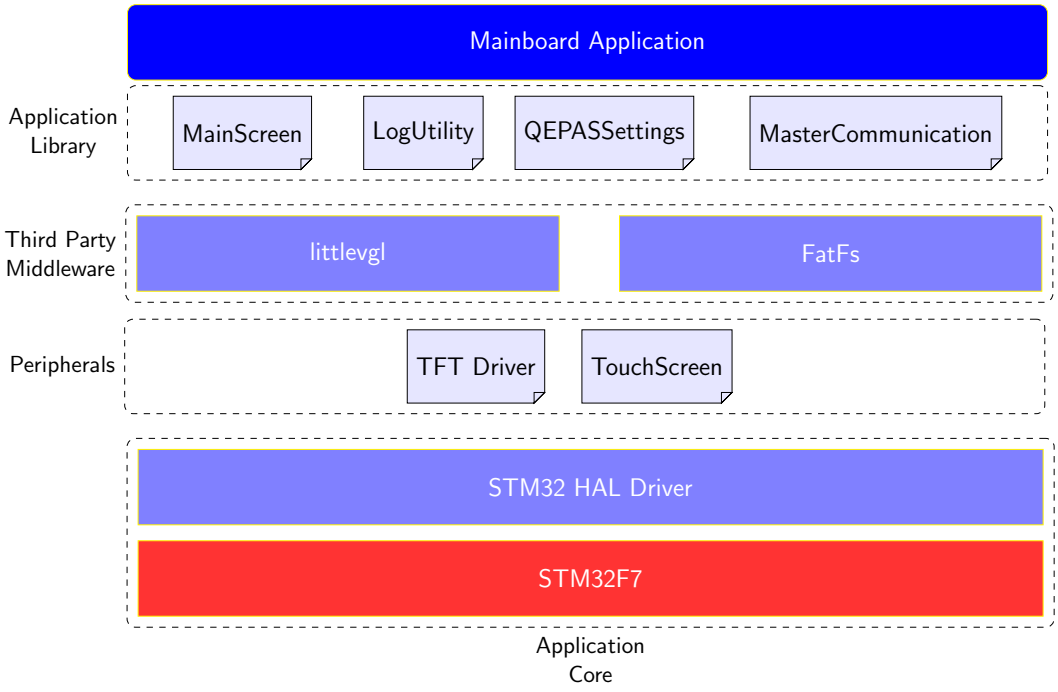

Figure 3.26: Overview of the mainboard firmware.

Visualization

The library LittlevGL provides different widgets and themes. For porting the library to the microcontroller and to use the display, there are a few functions in the API which must be adapted. These functions are responsible for the initialization of the display and writing the display contents to the

display. To use the touchscreen with the library, a callback function must be implemented. This callback is periodically executed by the library to check if there are inputs from the touchscreen. The TouchScreen class provides the functionality for initialization, interrupt configuration, reading of the X and Y coordinates with an internal ADC. This class uses the singleton design pattern since there are is only one touchscreen.

The layout and configuration of the widgets are done with the MainScreen class. To update the measurement values, the class has methods for this. There is a button to start and stop the measurements.

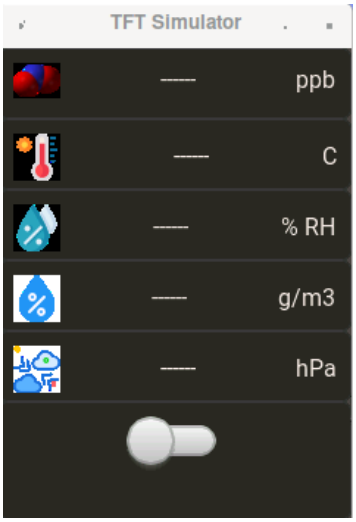

Figure 3.27: Appearance of the screen.

Logging

With the LogUtility class, the measurements can be logged on the SD-card. The class creates log files on the SD-card and logs the measurement values with a time stamp. After 86400 log entries, which is one day if the log interval is one second, a new log file is created.

The log files are stored in a CSV-format with a tab as delimiter.

The logging is activated/deactivated when the start/stop button is pressed.

Communication

The Mainboard acts as Master for the Control-and-Sensor Board. In the Mainboard firmware, the communication protocol, as discussed in section 3.3.1, is implemented. Therefore the MasterCommunication class provides methods to read and set parameters or to execute commands.

For the communication over the USB interface, an ASCII based communication protocol was used. The usage of an ASCII based protocol allows configuring the settings over a terminal application. Compared to the binary protocol for the RS485 interface, there is more overhead due to the ASCII representation, but this no problem in this application since there are only commands to modify parameters and download logged data which are not time critical.

The syntax for the ASCII protocol is given by follow Backus normal form:

```
message ::= (read_parameter_command | action_command) newline
read_parameter_command ::= "?" parameter_name
action_command ::= "!" (command | command ":" parameter_name ":"
    number | command ":" character+)
command ::= letter+
parameter_name ::= character+
character ::= letter | digit | "."
number ::= digit+ ("." digit+)?
digit ::= "0" | ... | "9"
letter ::= ("A" | ... | "Z") | ("a" | ... | "z")
newline ::= \n
```

Each message is terminated with \n. If the command is unknown, the Mainboard response is "unknown command". In case the format of the parameter set/read command is wrong, the response of the Mainboard is "invalid request".

Message examples:

- set parameters
  message: "!set:backgroundsamples:5\r \n"
  message: "!set:sweepstep:0.5\r \n"

- read parameters
  message: ”?sweepstart\r \n”
- list files
  message: ”!listfiles\r \n”
- download file
  message: ”!download:log122020_1430.csv\r \n”

Each byte of the message is stored into an array in an interrupt service routine (ISR). If a newline character was received in the ISR, a flag is set. This flag is checked in the main loop. Is the flag set, then the new message was processed and a response was sent.

Main Application

The tasks of the Mainboard are processing touch events, start/stop the measurement cycle of the CSB, visualization and logging of the measurement data.

During the startup of the mainboard firmware the peripherals are initialized. After that, the settings are read from the SD-card.

To react to touch events, the touch_handler method of the touchScreen class is called in each loop. Also, the lv_task_handler function from the LittlevGL library is called in each loop. This function is responsible for redrawing the UI.

As described earlier, the processing of new messages from the USB interface is done in the main loop. The function handle_master_message processes these messages and stores or reads the settings.

To control the measurement cycle, a state machine with 4 states is executed in the main loop. The state machine is shown in fig. 3.28. The initial state of the state machine is the idle state. If the start/stop button pressed, the state machine switches to the Start Measurement State. In this state, a new log file is created. The settings (see. section 3.3.1) are written to CSB. After the settings transferred, the Start Measurement Command is written to the CSB, and the CSB starts with the measurement cycle. The state machine switches into the Measurement On state.

In the Measurement On state, each incoming measurement data from the CSB is logged by the LogUtility class with the current time.

The useful signal is computed with equation (3.18), the background signal is vectorially subtracted from the measured signal, i.e. the in-phase part of the background signal is subtracted from the in-phase part of the measured signal and likewise for the quadrature signals. Due to the linear relationship between useful signal and analyte concentration, it is sufficient to subtract the useful signal by a certain offset and multiply by a gain (cf. equation (3.19)). The determination of the gain and offset is described in Chapter 4.

$$\text{magnitude} = (I - I_{\text{background}})^2 + (Q - Q_{\text{background}})^2 \tag{3.18}$$

$$\text{concentration} = \frac{\text{magnitude} - \text{offset}}{\text{gain}} \tag{3.19}$$

This state is executed until the start/stop button is pressed again. The state machine switches to the Stop Measurement state. This state stops the logging by saving the currently opened logfile. The Stop Measurement Command is written to the CSB. The values on the display are reset. Finally, the state machine switches to the Idle state.

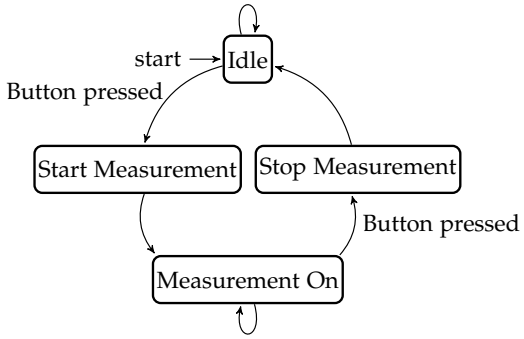

Figure 3.28: State Machine in the main loop.

3.3.3 Software

To interact with the Control-and-Sensor Board and the mainboard over its communication interfaces via a PC, two small applications are written with the QT framework.

The first application is the QEPAS Sensor Tool. The purpose of this application is to adjust the settings on the mainboard and to download the log files. It implements the ASCII protocol, which was covered in section 3.3.2.

The QEPAS Sensor Tool is shown in fig. 3.29.

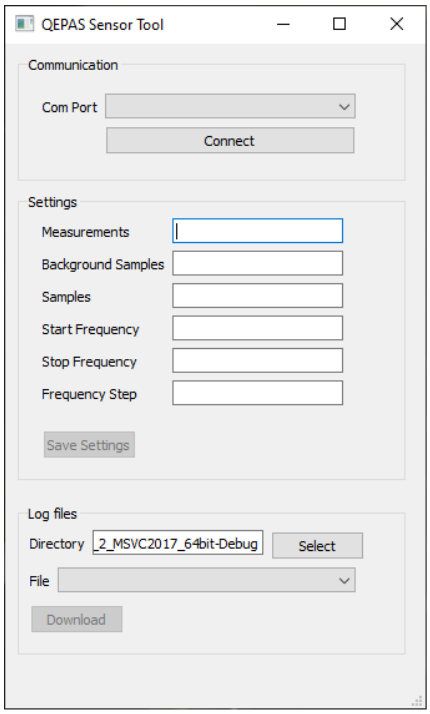

Figure 3.29: With the QEPAS Sensor the settings can be modified and logfiles can be downloaded.

With the QEPAS Service Tool (fig. 3.30), the Control-and-Sensor Board can be directly controlled over the RS485 interface. This application allows the user to modify the settings and provides different options in which mode the

CSB operates. In addition to the normal measurement mode, the following modes can be used

- Record Raw Data
  In this mode, the CSB fetches 25000 samples from the four ADC channels. This is done by sending the Raw Data command to the CSB. After this samples obtained, they transfered to the application. This mode is intended for test/verification purposes.
- Sweep
  The purpose of this mode is to find the resonance frequency of the QTF. It executes the Frequency Sweep state on the CSB.
- Run Calibration
  This mode obtains the specified samples for each calibration point. The number of calibration points can be set with the Calibration Points Input Box. The calibration mode can be used to record I and Q signals at different gas concentrations for calibration/verification purposes.

The tool shows the received data in a table view. It is also possible to log the received data.

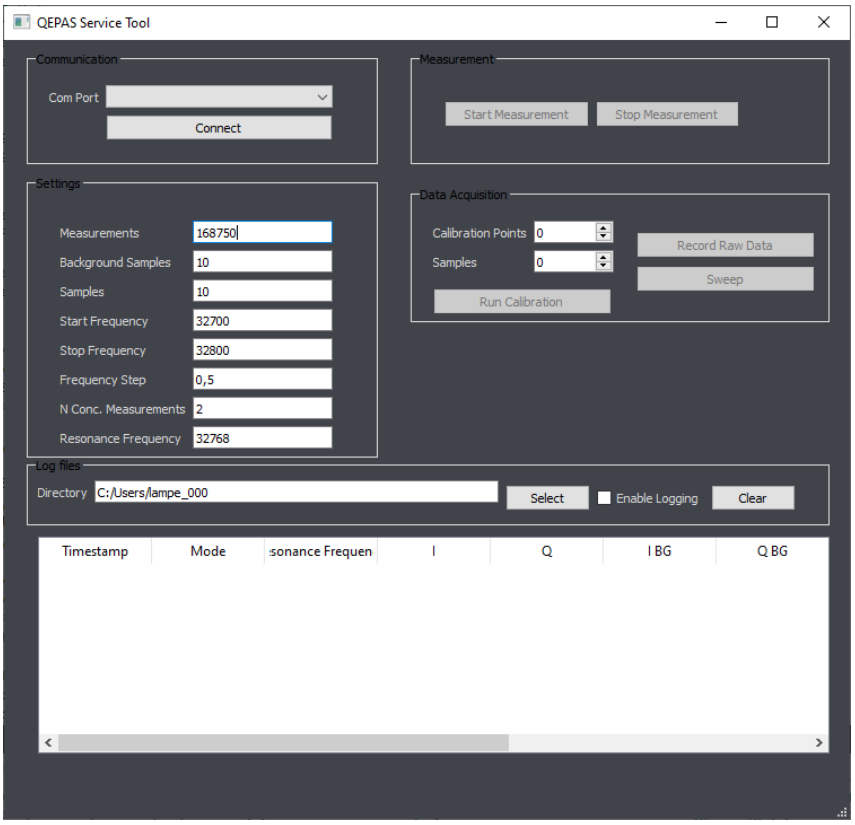

Figure 3.30: QEPAS Service Tool.

4 Results and Discussion

In this chapter, the results of the developed system are discussed. Furthermore, the measurement setup, which was used to evaluate the system is described. To evaluate the system, different concentrations were measured. With the measurements, the linearity and accuracy investigated. The limit of detection can be used to quantify the system in terms of applicability for certain applications, such as the measurement of NO_2 in urban areas. Finally, the influence of the laser driver on the limit of detection was evaluated.

4.1 Measurement Setup

The measurement setup is shown in fig. 4.1. It consists of a gas diluter, the cell with the optic system (fig. 4.2) and the developed electronics (fig. 4.3).

A gas diluter, which was developed in ref. [7], was used to create the gas concentrations. This diluter was connected to a nitrogen dioxide and synthetic air and allows to creating dilution rations down to 1:1400. To adjust the flow through the cell, a massflow controller (MFC) is used after the diluter. For the measurements the massflow is set to 0.5 l/min.

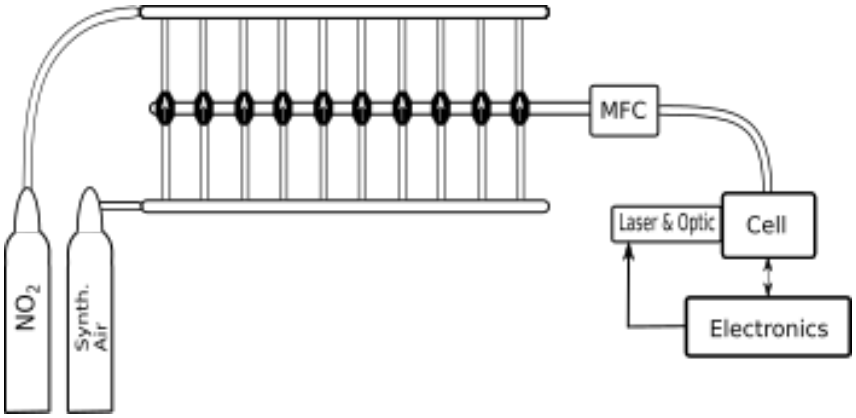

Figure 4.1: Labor setup for the evaluation of the sensor. NO_2 and Synthetic air are connected to a gas diluter. The mass flow controller controls the gas flow into the cell.

Beneath the cell is the PCB with the amplifier circuit and the QTF. The laser diode (OSRAM PL450B), with an emission wavelength of 450 nm, is used as a light source. The light is focused through the optical system between the prongs. The laser diode is driven by the IP250 laser driver and the amplified signal from the QTF is connected to CSB.

The metal cell is connected with the earth in the laboratory setup to reduce the impact of electromagnetic inference.

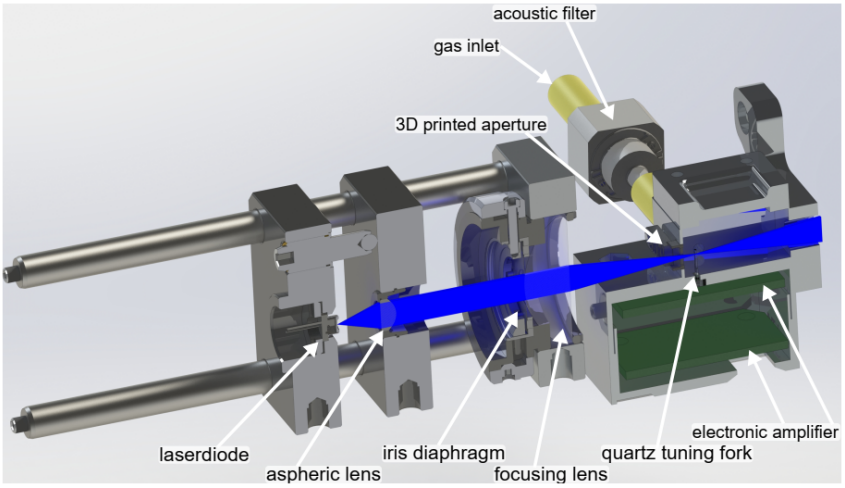

Figure 4.2: The cell and its optical setup [5].

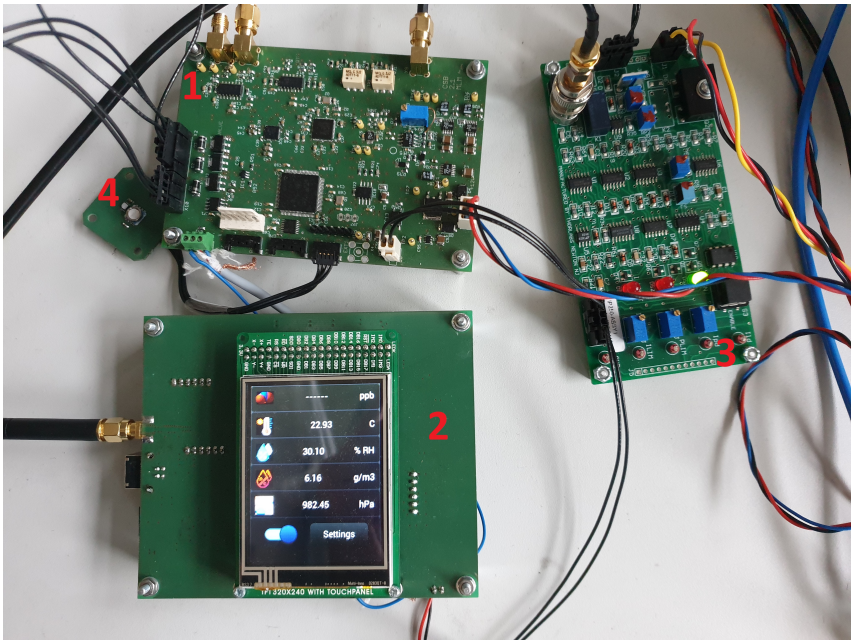

Figure 4.3: The complete system is shown in this figure. (1) Control-and-Sensor Board, (2) Mainboard, (3) Laserdriver IP250, (4) HTB Board.

4.2 Calibration

A linear model was used in this thesis to compute the concentration from the signal amplitude of the QTF. The relation between the magnitude and the concentration can be expressed with

$$\text{magnitude} = \text{gain} \cdot \text{concentration} + \text{offset} \tag{4.1}$$

Rewriting eq. 4.1, the concentration can computed with

$$\text{concentration} = \frac{\text{magnitude} - \text{offset}}{\text{gain}} \tag{4.2}$$

The values of these parameters are obtained with a calibration routine. The calibration routine is implemented in the QEPAS Service Tool. During the calibration routine, samples of different concentrations are recorded. The calibration points are shown in tab. 4.2. Before the concentration samples were recorded, the background signal was recorded. For each calibration point a file with samples was created by the Service Tool. A Matlab script reads all files and post-processes the data. For each concentration, the background signal is vectorially subtracted and the magnitude was computed. After this post-processing steps, a linear fit was applied to data to obtain the gain and offset parameters. The results of this line fit and the used fitting procedure can be found in section 4.3.

Calibration Point	Samples
synthetic air	60
0.606 ppm	60
synthetic air	60
1.911 ppm	60
synthetic air	60
4.263 ppm	60
synthetic air	60
9.72 ppm	60
synthetic air	60
13.71 ppm	60
synthetic air	60
19.20 ppm	60

Table 4.1: calibribation points and number of samples for each calibration point

4.3 Concentration Meaurements and Linearity

The results of the concentration measurements are shown in fig. 4.4. The measured concentrations are in the range from 0 ppm up to 19.2ppm. The blue curve shows the amplitude after the lock-in amplifier and the background subtraction. The orange curve shows the concentration, which was set with the gas diluter.

From fig. 4.4 it can be observed that there is a short delay at each gas concentration step. A delay is caused by the mean filter. The mean filter can described as FIR filter (eq. (3.8)). For a FIR filter the group delay is given

$$\tau_g = \frac{N-1}{2}T \tag{4.3}$$

The mean filter averages over N=168750 samples at a sampling period T of $\frac{1}{167850\text{Hz}}$. With these parameters, the mean filter has a group delay τ_g of 0.5 s.

Another source, which influences the delay comes from the measurement setup. It takes some time until the gas is exchanged and replaced the old gas concentration in the laboratory setup. The gas concentration is set by hand and the measurement continued manually in the Service Tool, which also causes a delay for each concentration.

Especially at 4.263 ppm and 13.71 ppm no delay can be observed, which can be caused by the manually adjust of the concentration.

In an overall view, the results of the concentration measurements match the concentrations well. There is also measurement noise at the concentrations. The measurement noise varies between a standard deviation of 0.0002 for 0 ppm and 0.0125 for 19.2 ppm. This increasing standard deviation is proportional to the uncertainties of the gas diluter. The standard deviations for the gas diluter are in the range of 0.010 ppm for 0 ppm and 0.29 ppm for 19.2 ppm. The measurement noise depends also on the amplifier stages in the electronics.

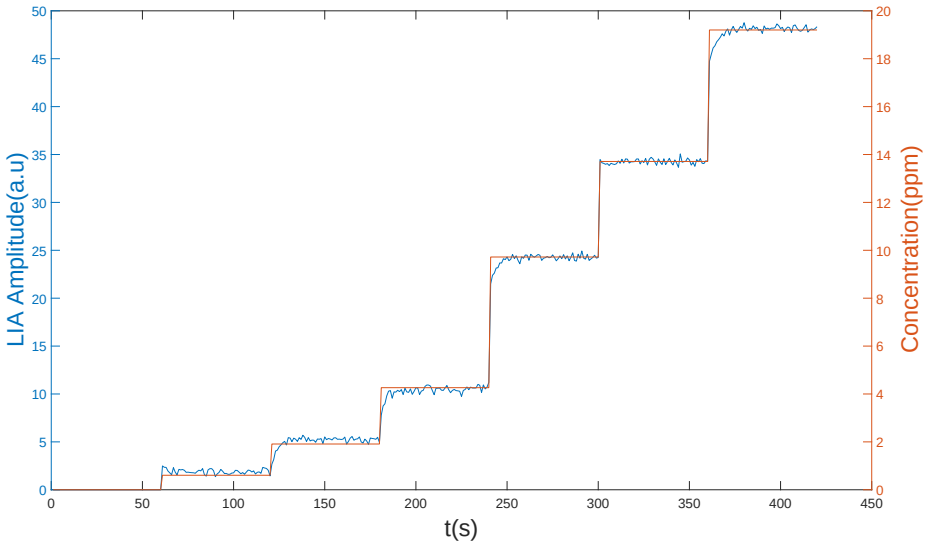

Figure 4.4: measurement of different NO_2 concentrations with 1s integration time.

As a fitting procedure, the approach described in ref. [23] was used in this thesis. The line fit assumes independent data points with normally

distributed errors in x and y. These errors are considered in the computation of the line parameters. The results of this line fit are shown in fig. 4.5.

The linear model assumption matches the recorded data points. In contrast to an ordinary least squares fit, the chosen fit function gives a slightly different slope. This results from the larger errorbars of the measurement points at higher concentrations, which in turn have a lower weight in the fit. This result shows a linear response of the sensor for different gas concentrations.

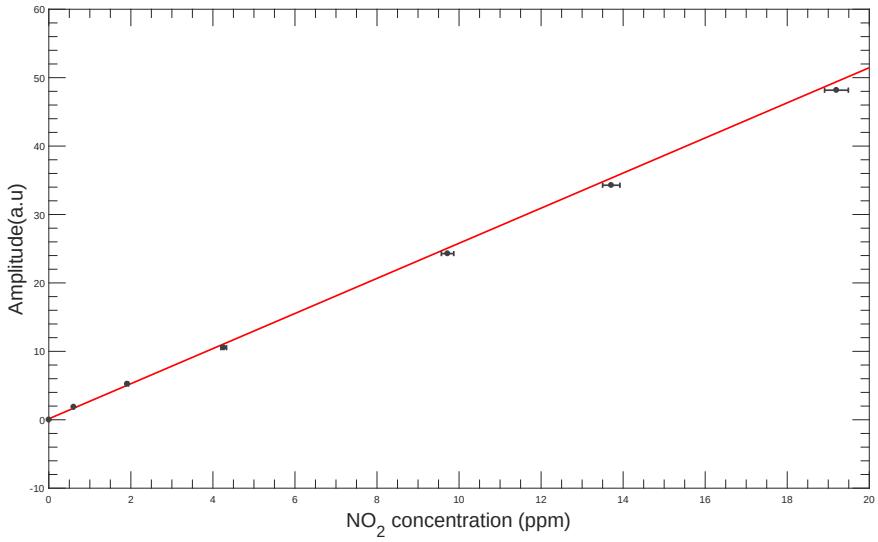

Figure 4.5: Comparision of the fitted line and the recorded amplitude. The standard error is represented with error bars in the QEPAS signal relatively to the mean. The errorbars for the amplitude are too small to be visiable on this scale .

4.4 Limit of Detection

To make a statement about the quality of the developed sensor, the limit of detection (LOD) is calculated and discussed. The limit of detection states the achievable resolution of the QEPAS sensor. For determining the limit of detection of the sensor, an Allan variance analysis was used in this work.

Originally, the allan variance method was used to measure the stability of frequency in oscillators and amplifiers. The usage of the Allan variance to determine the limit of detection was proposed in Ref [19].

This method is based on the measurement of zero air, which does not contain the target substance. The measurements are done with synthetic air for one hour and from this recordings the Allan variance was computed with a Matlab script. The signal is recorded with the low cost Thorlabs IP250 laser driver and is shown in fig. 4.6. To compare the results of the developed QEPAS sensor with the system described in Ref. [5], which was based on a National Instruments PXI system and a high cost Thorlabs ITC4001 laser driver, the background signal is also recorded with the ITC4001 laser driver (fig. 4.7).

The computed Allan variance is based on the magnitude, to convert it to the concentration, the result of the Allan variance is divided by the gain.

The limit of detection can now found by

$$LOD = min\ \sigma(M, T, \tau) \tag{4.4}$$

where $\sigma(M, T, \tau)$ denotes the Allan variance. The limit of detection is given by the minimum of the Allan variance. Fig. 4.8 shows the Allan variance for the IP250 and fig. 4.9. the Allan variance for the ITC4001.

With the IP250 a LOD of 48 ppb and the ITC4001a LOD of 27 ppb can be achieved. Another quantity of interest is the integration time, which is required to achieve the LOD. This can be found by considering

$$arg\ \min_{\tau}\ \sigma(M, T, \tau) \tag{4.5}$$

The optimal integration time is 18 s for the IP250 and 58 s for the ITC4001.

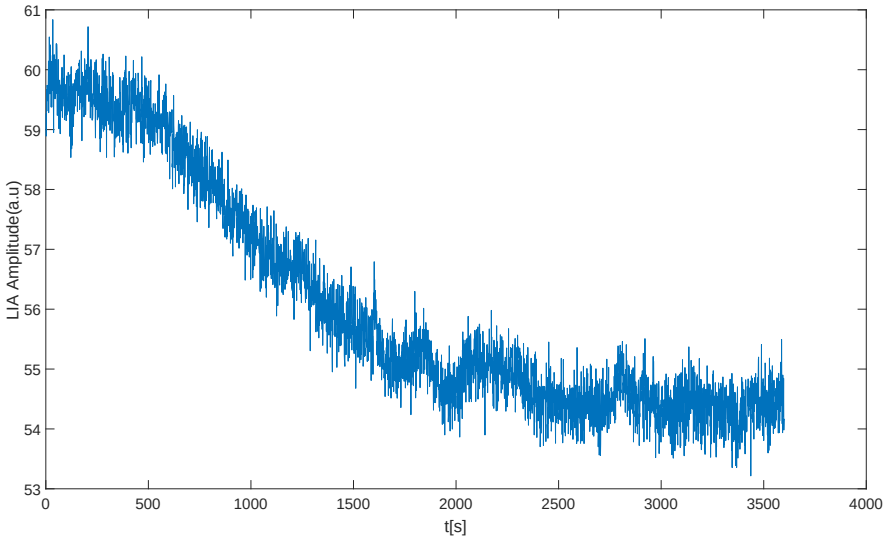

Figure 4.6: Background measurement measured with Laser Driver IP250.

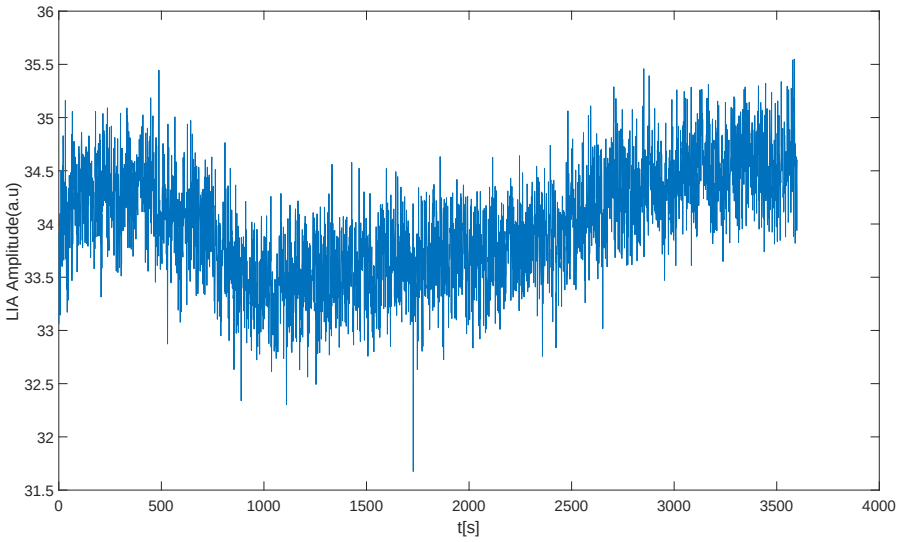

Figure 4.7: Background measurement measured with Laser Driver ITC4001.

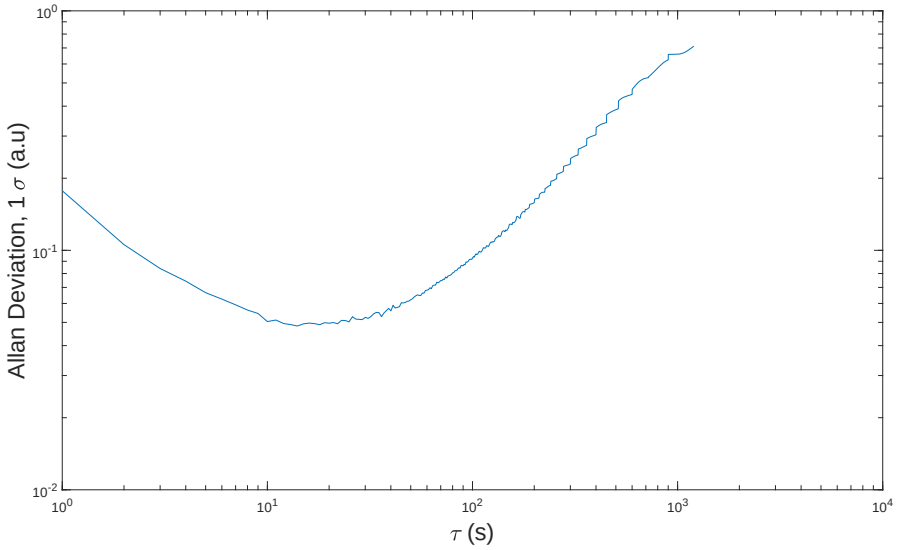

Figure 4.8: Allan Deviation of the background signal with IP250.

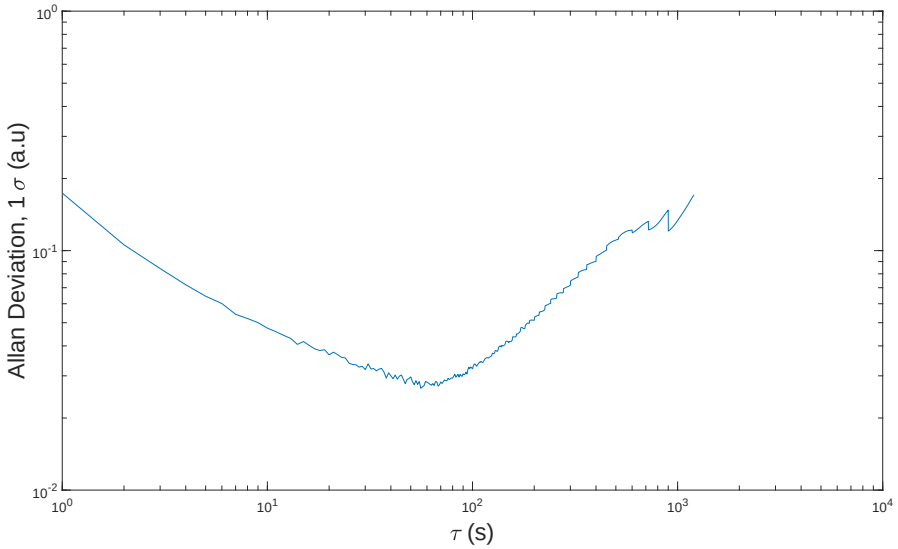

Figure 4.9: Allan Deviation of the background signal with ITC4001.

The achieved results are very good as compared to the setup described in Ref [5], which used a much higher cost solution. In [5] and the setup developed in this thesis, the LOD was 21 ppb for an integration time of 80 s. With the ITC4001,the LOD is 27 ppb, which is close to the referenced system. In the recorded background signal with the ITC4001, a small signal drift can be observed. This drift prevents that a better LOD was achieved. This drift reduces the possible averaging time because the Allan variance starts to increase earlier. With the developed low-cost sensor, it is possible to achieve a similar LOD as compared to a high-cost data acquisition system.

In terms of the maximum achievable LOD, the low-cost laser driver (IP250) only performs half as good as the high-cost laser driver. A reason for the worse performance of the IP250 is the large drift in the background signal. This drift has a large impact on the integration time and the LOD. Since both laser drivers show a drift in the background signal, this drift is further investigated in the next chapter.

4.5 Drift and Laser Driver Evaluation

To exclude that the drift is caused by the electronics, a sinusoidal input signal with the same frequency as the reference signals were applied to the lock-in amplifier. This measurement ran for two hours and the result is shown in fig. 4.10. Besides the measurement noise, no drift can be recognized.

Both laser drivers have run for one hour with synthetic air. Additionally, the laser power was recorded with a power meter. The laser power and the result of the lock-in amplifier for each laser driver is plotted in figure 4.11. The same result as earlier has been observed, namely that the IP250 shows a large drift as compared to the ITC4001.

The trend of the signal from the lock-in amplifier and the power meter signal matches for both laser drivers. There is a correlation between the lock-in amplifier signal and the power signal, which means the drift is caused by the modulation signal from the laser driver.

In the product specification, the manufacturer specifies a current drift $<$ 100 uA in a time interval of 30 min for the IP250. For the ITC4001, a current

drift < 100 µA is stated for a time of 24 hours. This is in line with our measurement results. Thus, it can be concluded that the laser driver has a significant impact on the limit of detection of the sensor.

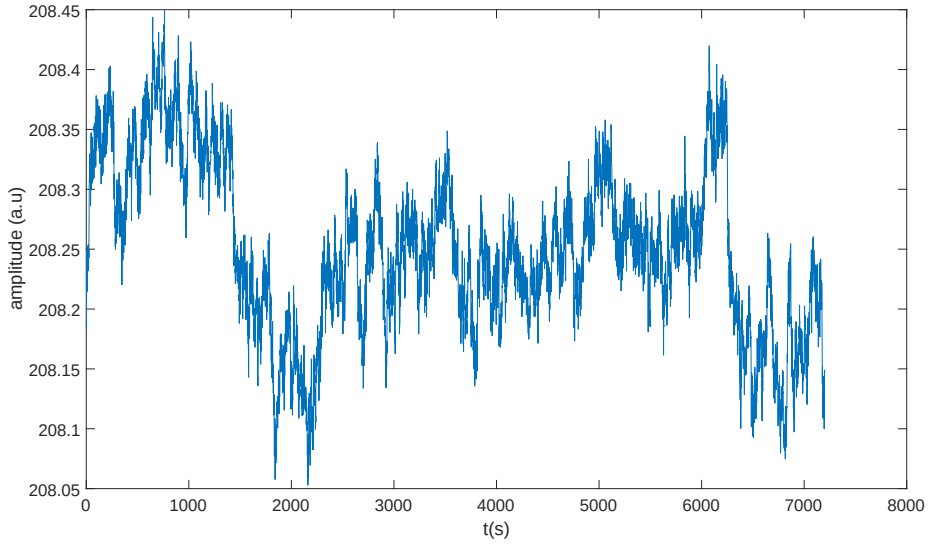

Figure 4.10: Measurement for 2 hours with a sinusoidal input signal from an frequency generator.

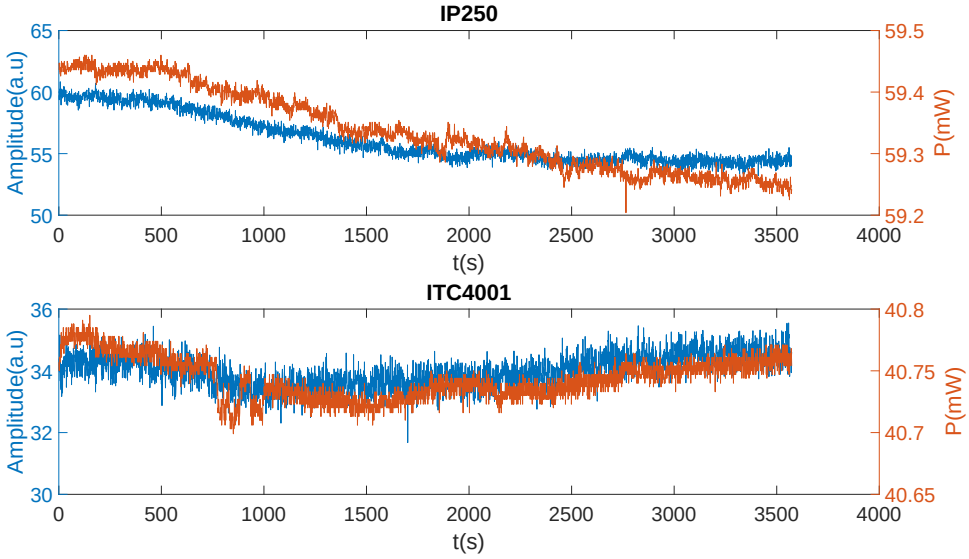

Figure 4.11: The Laser Power of ITC4001 and IP250 in comparision to corresponging background signal.

5 Conclusion and Outlook

A sensor for NO_2, based on quartz-enhanced photoacoustic spectroscopy, was developed within in this thesis. Air pollutants have an impact on the health and the environment. Current available sensors for NO_2 have major drawbacks, either high cost or they suffer from low accuracy. This work uses the quartz-enhanced photoacoustic spectroscopy, which is immune to environmental noise and allows it build a compact sensor.

The developed system consists of hardware and firmware. The core part of the hardware is the Control-and-Sensor board, which generates the reference signals with a DDS for the lock-in amplifier and carry out the data acquisition with a $\Delta\Sigma$-ADC of the reference signals and the signal from the quartz-tuning fork. The lock-in amplifier runs as firmware in a microcontroller. The implementation in the firmware allows the user to adjust the lock-in amplifier. A state machine was developed in the firmware to control the measurement cycle. The firmware uses an RS485 interface for parametrization and transmission of the measurements. The second part of the hardware is the Mainboard, which is responsible for the visualization and logging the measurements. The measurements are logged on a SD-card, which is connected via a parallel interface to the microcontroller. The visualization is build on top of the embedded graphics library LVGL. The Mainboard provides two interfaces, a RS485 interface for the communication with the Control-and-Sensorboard and a USB Interface for configuration purposes. Two software applications were developed with the QT framework to control and configure the Mainboard and Control-and-Sensorboard.

The developed system is evaluated with a laboratory setup. In this setup, different concentrations of NO_2 used for measurements with the sensor. The linearity of the sensor is verified with the measurements. The limit of detection of the system is calculated for two laser drivers. With the

low-cost laser driver IP250, a LOD of 48 ppb and with the high-cost laser driver ITC4004, a LOD of 27 ppb can be achieved. The integration time for the IP250 is 18 s and for the ITC4001 is 58 s to get to the LOD. During the measurements, a drift was observed for both laser drivers. Further investigations have shown that the drift stability of the laser drivers has a significant impact on the limit of detection.

As was shown in this work, the system can achieve a sufficient detection limit, which makes the system usable for monitoring NO_2 in urban areas. Future efforts towards a QEPAS-based low-cost sensor should focus on the laser driver, temperature control inside the measurement chamber, signal processing improvements, data transmission over long distances and the device housing.

To reduce the temperature influence on the measurement Peltier elements can be used to control the temperature inside the measurement chamber. Therefore, an integration of a Peltier control circuit would be an improvement for the measurement. The Peltier element can also be used for the temperature stabilization of the laser diode to prevent thermal drift. With a pump, the gas exchange in the measurement chamber would be faster, which reduces the time between measurements and make it possible to track the evolution of the NO_2 better.

The current setup was only used with commercial laser drivers. The requirements for the laser are high to obtain a sufficient detection limit with the sensor. Therefore, future works should focus on the development of a custom laser driver, which is able to fulfill the requirements of this application. Another possibility for improvement is the adaption of the digital filters, which are applied to the magnitude from the lock-in amplifiers. This may lead to a reduction of the integration time and even a better detection limit. Another interesting feature is the application of air quality sensors in wireless sensor networks. Continued development of the sensor may integrate low-power wide-area network connectivity, e.g. Long Range (LoRa), to transmit the measurement data. Finally, a housing witch includes all necessary components and allows an effortless placement of the measurement system would increasing usability. A field test is also necessary to test the system under real conditions and to identify weak spots and solve them with further development.

List of Figures

Bibliography

[1] alphasense. *NO2-A43F*. URL: http://www.alphasense.com/index.php/products/nitrogen-dioxide-2/ (cit. on p. 6).

[2] AMSYS. *MS5803-02BA Miniature Altimeter Module*. 2013. URL: https://www.amsys.de/downloads/data/MS5803-02BA-AMSYS-datasheet.pdf (cit. on p. 33).

[3] Jean-Philippe Besson. *photoacoustic spectroscopy for multi-gas sensing using near infrared lasers*. 2006 (cit. on p. 7).

[4] Zoltán Bozóki, Andrea Pogány, and Gabor Szabo. "Photoacoustic Instruments for Practical Applications: Present, Potentials, and Future Challenges." In: *Applied Spectroscopy Reviews* 46 (Jan. 2011), pp. 1–37. DOI: 10.1080/05704928.2010.520178 (cit. on p. 7).

[5] P. Breitegger. *Low Cost Sensing Technologies for Monitoring Air Pollutants in Metropolitan Areas*. 2020 (cit. on pp. 57, 62, 65).

[6] P. Breitegger et al. "Towards Low-Cost QEPAS Sensors for Nitrogen Dioxide Detection." In: *Photoacoustics* (2020), p. 100169. ISSN: 2213-5979. DOI: https://doi.org/10.1016/j.pacs.2020.100169. URL: http://www.sciencedirect.com/science/article/pii/S2213597920300094 (cit. on p. 12).

[7] Philipp Breitegger and Alexander Bergmann. "A Precise Gas Dilutor Based on Binary Weighted Critical Flows to Create NO2 Concentrations." English. In: *A Precise Gas Dilutor Based on Binary Weighted Critical Flows to Create NO2 Concentrations*. Vol. 2. Proceedings. MDPI AG, Dec. 2018, pp. 1–4. DOI: 10.3390/PROCEEDINGS2130998 (cit. on p. 55).

[8] Analog Devices. *AD9958 Datasheet Rev C.* 2016. URL: https://www.analog.com/media/en/technical-documentation/data-sheets/AD9958.pdf (cit. on p. 15).

[9] FTDI. *FT232BM Designers GuideVersion 2.0*. 2002. URL: https://www.ftdichip.com/Support/Documents/AppNotes/DG232_20.pdf (cit. on p. 28).

[10] Zurich Instruments. *Principles of lock-in detectionand the state of the art*. 2016. URL: https://www.zhinst.com/sites/default/files/li_primer/zi_whitepaper_principles_of_lock-in_detection.pdf (cit. on pp. 8, 10).

[11] A. A. Kosterev et al. "Quartz-enhanced photoacoustic spectroscopy." In: *Opt. Lett.* 27.21 (Nov. 2002), pp. 1902–1904. DOI: 10.1364/OL.27.001902. URL: http://ol.osa.org/abstract.cfm?URI=ol-27-21-1902 (cit. on pp. 7, 8, 13).

[12] Richard G. Lyons. *Understanding Digital Signal Processing*. 3rd Edition. Amsterdam: Pearson Education, 2010. ISBN: 978-0-137-02852-8 (cit. on p. 37).

[13] ST Microelectronics. *AN2790 TFT LCD interfacing with the high-density STM32F10xxx FSMC*. 2008. URL: https://www.st.com/content/ccc/resource/technical/document/application_note/85/ad/ef/0f/a3/a6/49/9a/CD00201397.pdf/files/CD00201397.pdf/jcr:content/translations/en.CD00201397.pdf (cit. on p. 25).

[14] World Health Organization. *WHO Air quality guidelines for particulate matter, ozone, nitrogen dioxide and sulfur dioxide*. 2005. URL: https://apps.who.int/iris/handle/10665/69477 (cit. on p. 1).

[15] Henry W. Ott. "Partitioning and Layout of a Mixed-Signal PCB." In: *Printed Circuit Desing Magazine* (June 2001), pp. 8–11 (cit. on p. 22).

[16] Pietro Patimisco et al. "Quartz-Enhanced Photoacoustic Spectroscopy: A Review." In: *Sensors (Basel, Switzerland)* 14 (Apr. 2014), pp. 6165–206. DOI: 10.3390/s140406165 (cit. on pp. 13, 44).

[17] ECO physics. *ECO PHYSICS nCLD 82 S Modular Gas Analyzer*. URL: https://www.ecophysics.com/industrial/modular-line/ncld-82-s/ (cit. on p. 4).

[18] NXP Semiconductors. *AN10675*. 2008. URL: https://www.nxp.com/docs/en/application-note/AN10675.pdf (cit. on p. 25).

[19] P. Werle, R. Mücke, and F. Slemr. "The limits of signal averaging in atmospheric trace-gas monitoring by tunable diode-laser absorption spectroscopy (TDLAS)." en. In: *Applied Physics B Photophysics and Laser Chemistry* 57.2 (Aug. 1993), pp. 131–139. ISSN: 0721-7269, 1432-0649. DOI: 10.1007/BF00425997. URL: http://link.springer.com/10.1007/BF00425997 (visited on 06/23/2020) (cit. on p. 62).

[20] Gerhard Wiegleb. *Gasmesstechnik in Theorie und Praxis - Messgeräte, Sensoren, Anwendungen*. Berlin Heidelberg New York: Springer-Verlag, 2016. ISBN: 978-3-658-10687-4 (cit. on pp. 3, 5, 6).

[21] Arthur Williams and Fred J. Taylor. *Electronic Filter Design Handbook, Fourth Edition* -. 004. Aufl. New York: McGraw-Hill Education, 2006. ISBN: 978-0-071-47171-8 (cit. on p. 15).

[22] *World Air Quality Index Project*. URL: http://aqicn.org/ (cit. on p. 1).

[23] Derek York. "LEAST-SQUARES FITTING OF A STRAIGHT LINE." en. In: *Canadian Journal of Physics* 44.5 (May 1966), pp. 1079–1086. ISSN: 0008-4204, 1208-6045. DOI: 10.1139/p66-090. URL: http://www.nrcresearchpress.com/doi/10.1139/p66-090 (visited on 06/23/2020) (cit. on p. 60).

Appendix

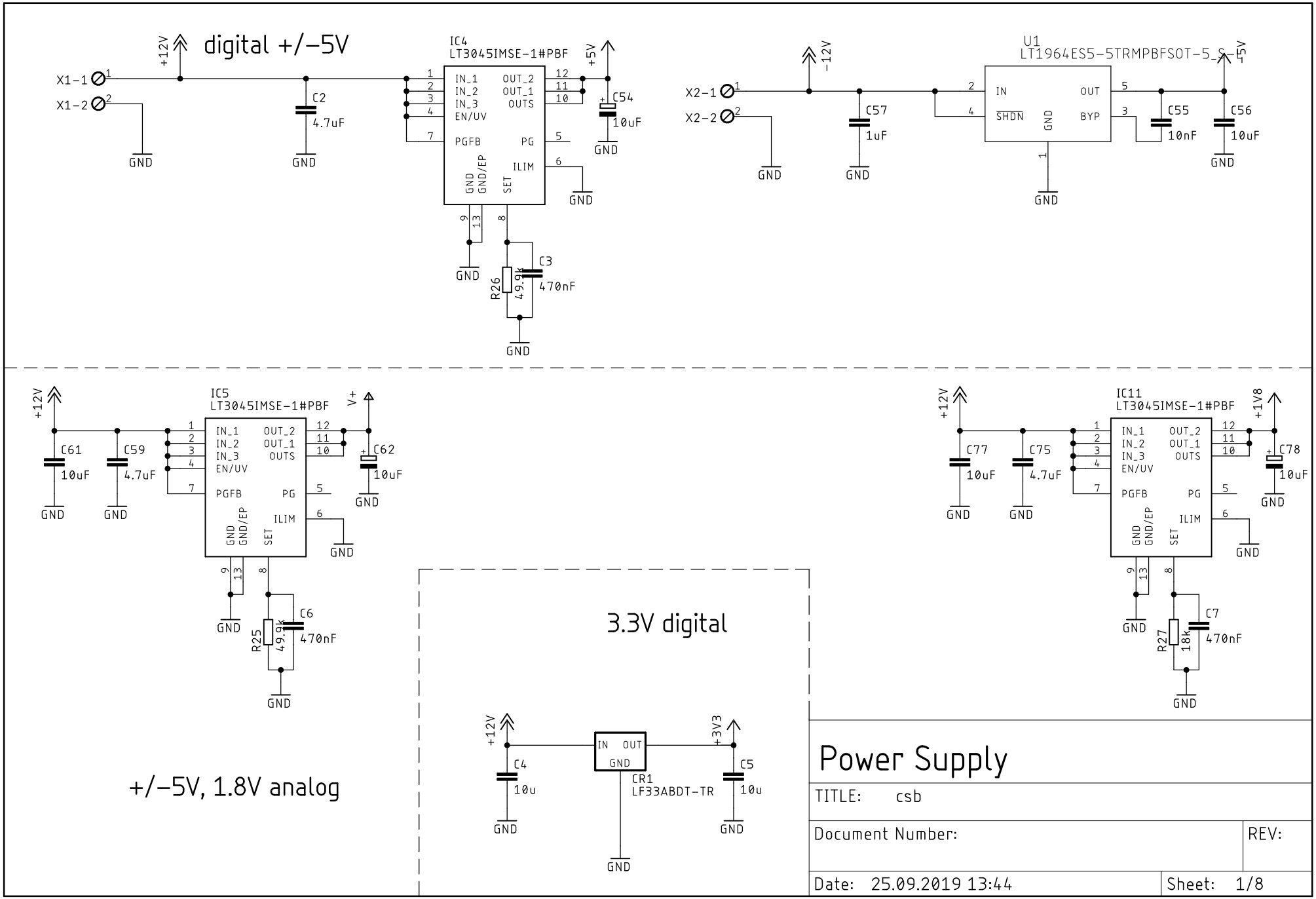
digital +/−5V
+12V
X1-1
X1-2
GND
C2
4.7uF
IC4
LT3045IMSE-1#PBF
IN_1
IN_2
IN_3
EN/UV
PGFB
GND
GND/EP
OUT_2
OUT_1
OUTS
PG
ILIM
SET
+5V
C54
10uF
R26
49.9k
C3
470nF
-12V
X2-1
X2-2
C57
1uF
U1
LT1964ES5-5TRMPBFSOT-5_S
IN
SHDN
GND
OUT
BYP
-5V
C55
10nF
C56
10uF
+/−5V, 1.8V analog
C61
10uF
C59
4.7uF
V+
C62
10uF
R25
49.9k
C6
470nF
3.3V digital
C4
10u
CR1
LF33ABDT-TR
+3V3
C5
10u
C77
10uF
C75
4.7uF
IC11
+1V8
C78
10uF
R27
18k
C7
470nF
Power Supply
TITLE: csb
Document Number:
REV:
Date: 25.09.2019 13:44
Sheet: 1/8

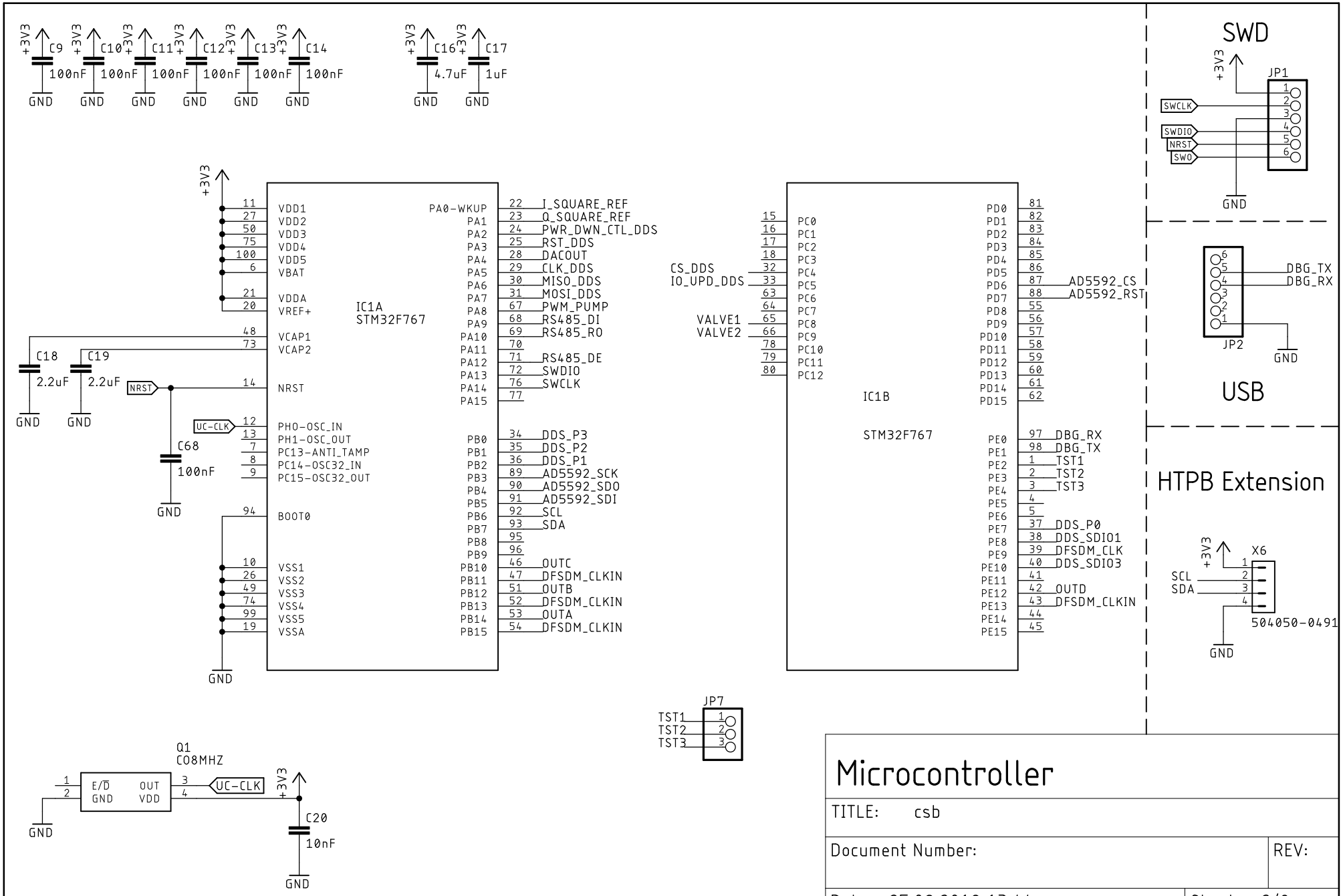

Microcontroller

TITLE: csb		
Document Number:		REV:
Date: 25.09.2019 13:44	Sheet: 2/8	

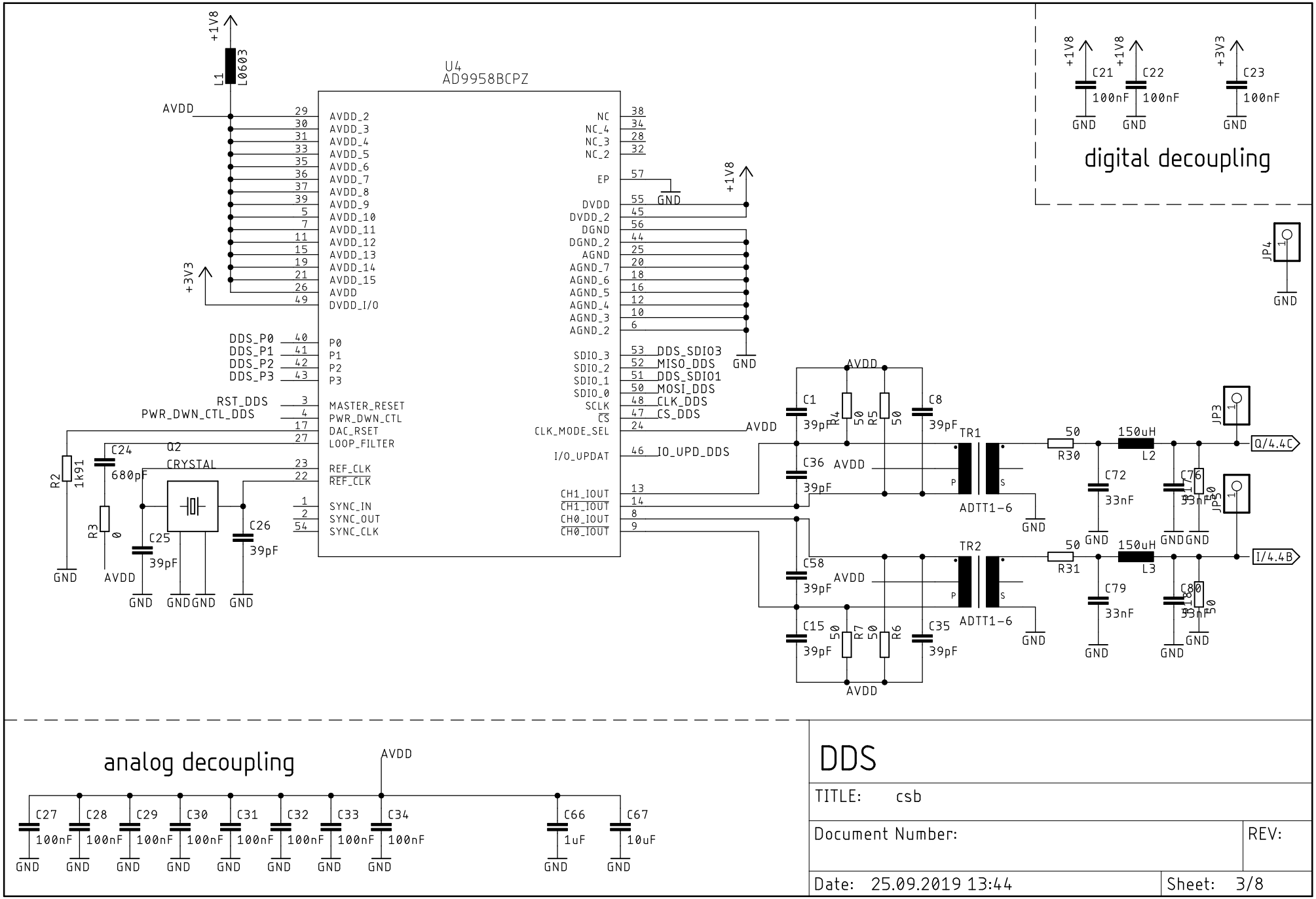

DDS

TITLE: csb

Document Number:

REV:

Date: 25.09.2019 13:44

Sheet: 3/8

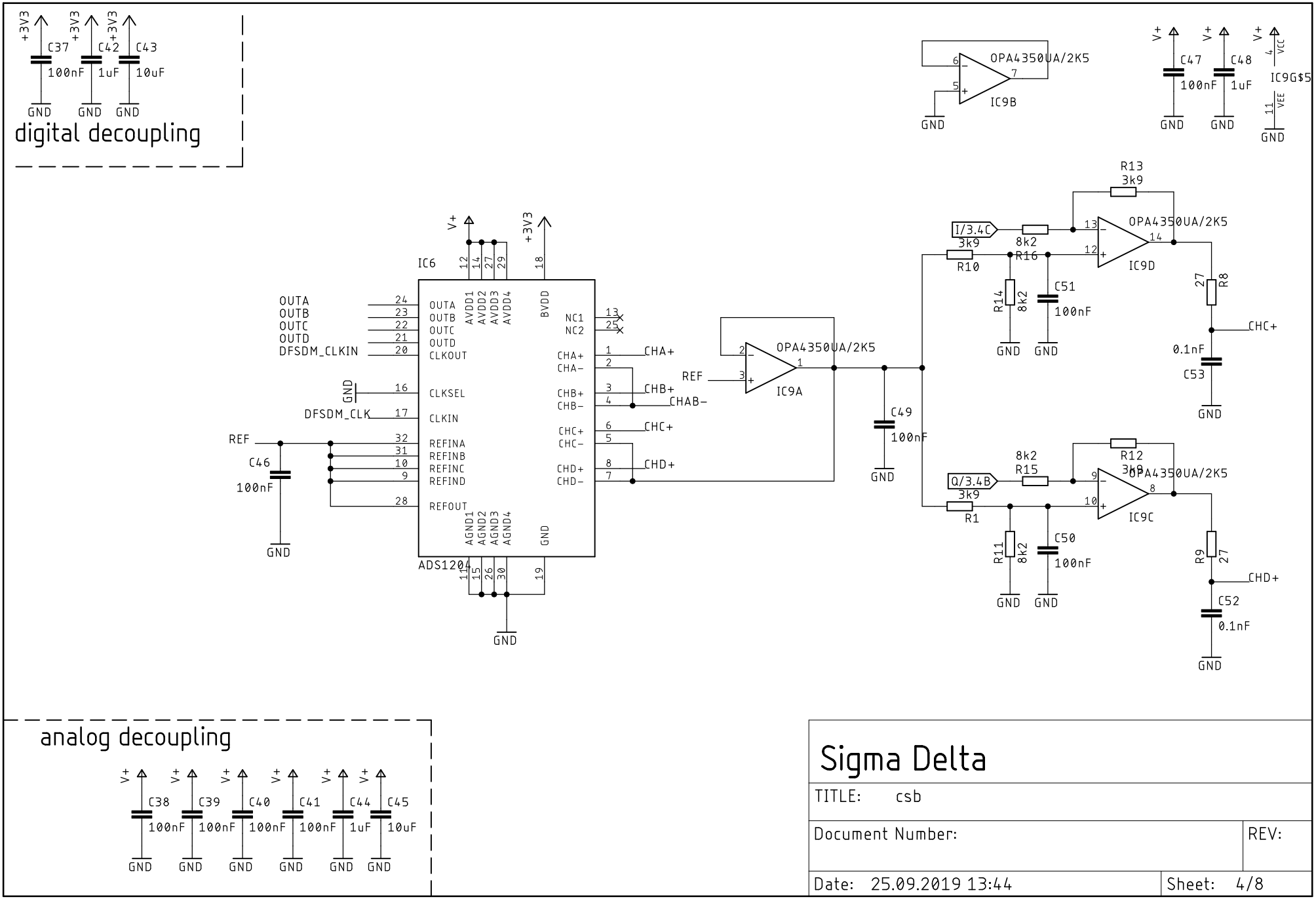
digital decoupling
+3V3
C37
100nF
C42
1uF
C43
10uF
GND
analog decoupling
V+
C38
C39
C40
C41
C44
C45
100nF
1uF
10uF
IC6
ADS1204
OUTA
OUTB
OUTC
OUTD
DFSDM_CLKIN
CLKOUT
CLKSEL
DFSDM_CLK
CLKIN
REFINA
REFINB
REFINC
REFIND
REFOUT
AVDD1
AVDD2
AVDD3
AVDD4
BVDD
AGND1
AGND2
AGND3
AGND4
NC1
NC2
CHA+
CHA−
CHB+
CHB−
CHC+
CHC−
CHD+
CHD−
CHA+
CHB+
CHAB−
CHC+
CHD+
REF
C46
100nF
IC9A
IC9B
IC9C
IC9D
OPA4350UA/2K5
C49
100nF
I/3.4C
Q/3.4B
3k9
8k2
R10
R16
R14
R13
R15
R1
R11
R12
C51
C50
R8
R9
27
0.1nF
C53
C52
C47
C48
IC9G$5
VCC
VEE
Sigma Delta
TITLE: csb
Document Number:
REV:
Date: 25.09.2019 13:44
Sheet: 4/8

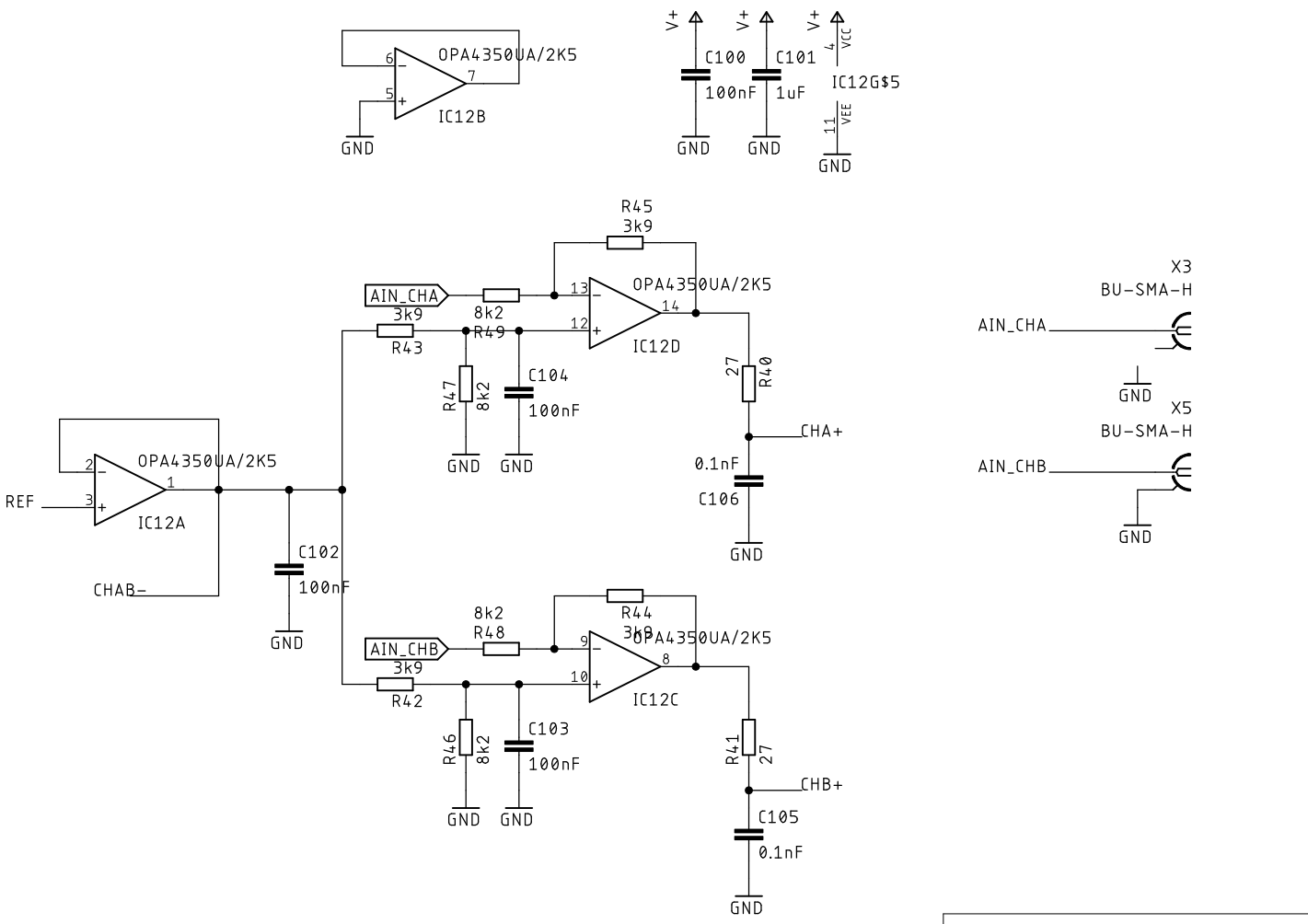

Sigma Delta Extern Input

TITLE: csb	
Document Number:	REV:
Date: 25.09.2019 13:44	Sheet: 5/8

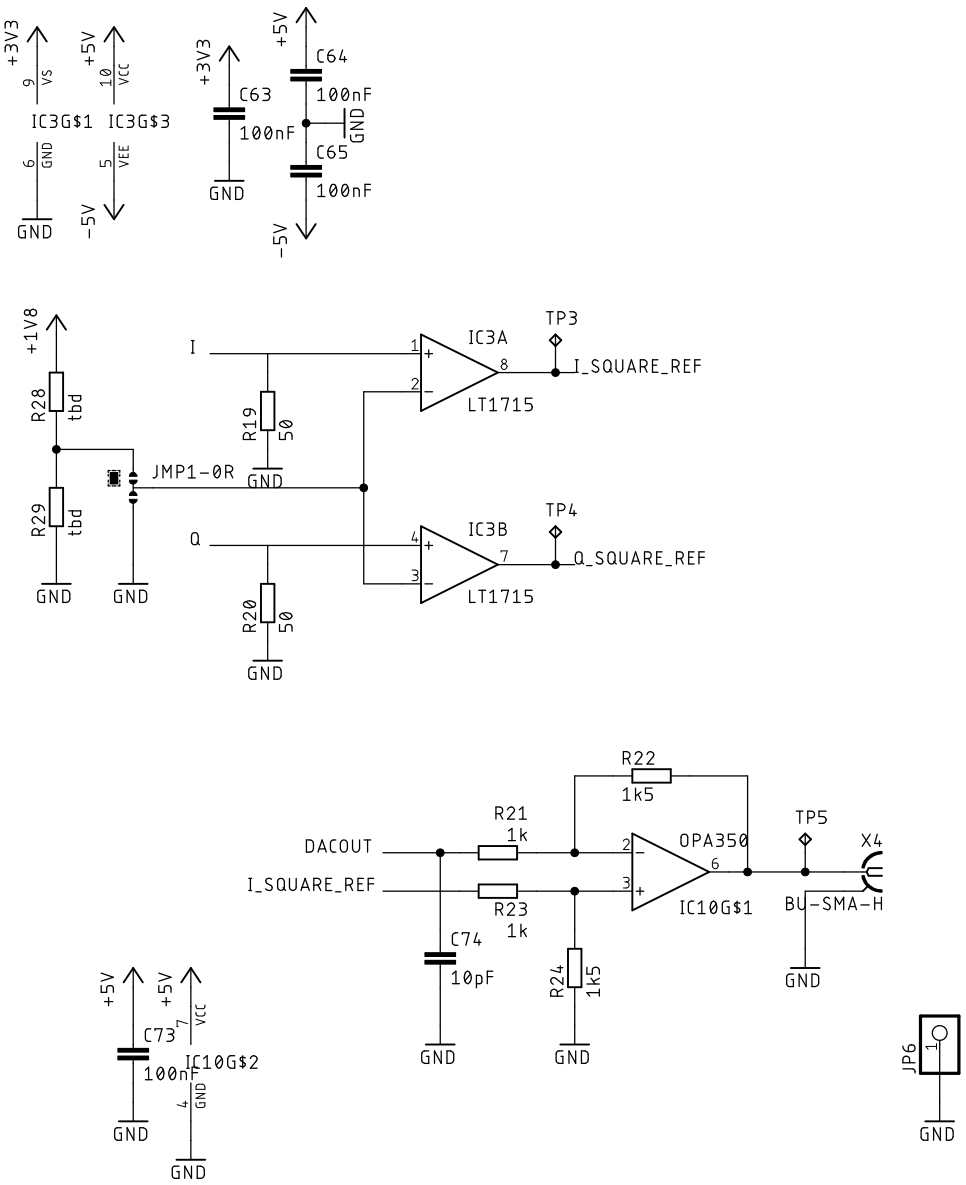

Square Wave Generation

TITLE: csb	
Document Number:	REV:
Date: 25.09.2019 13:44	Sheet: 6/8

Extension Interface

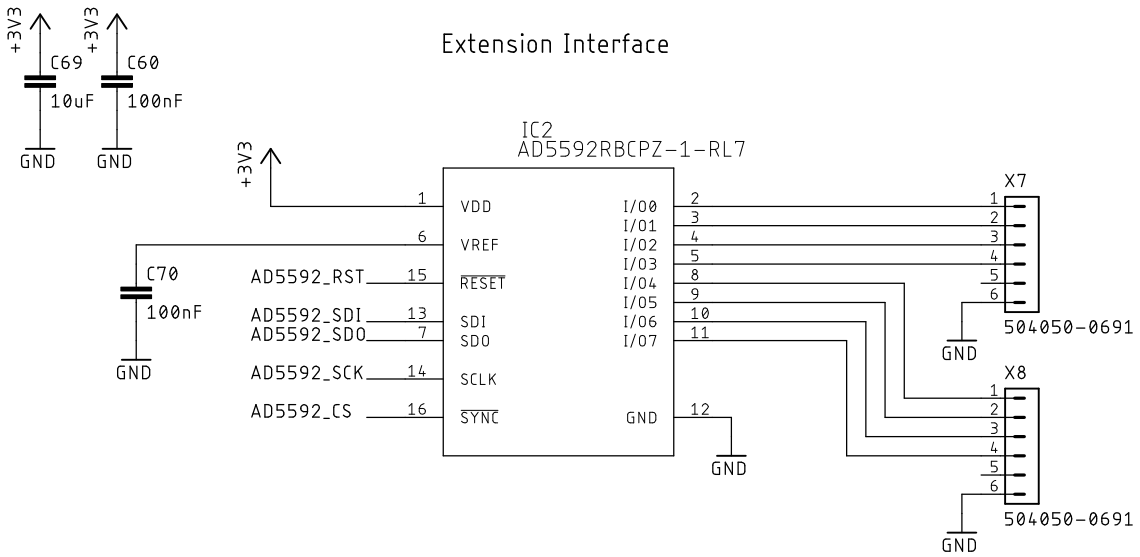

MB Interface RS485

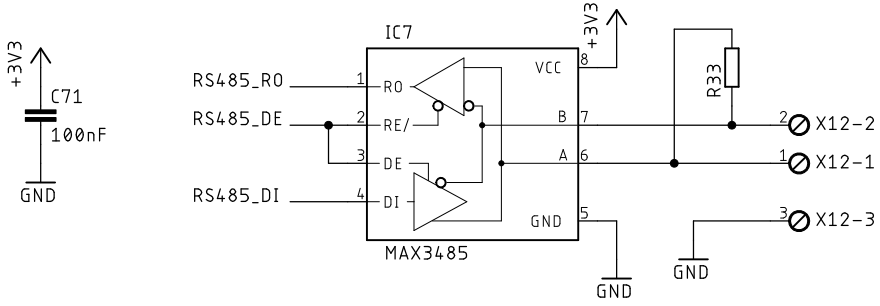

Interfaces

TITLE: csb	
Document Number:	REV:
Date: 25.09.2019 13:44	Sheet: 7/8

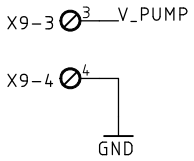

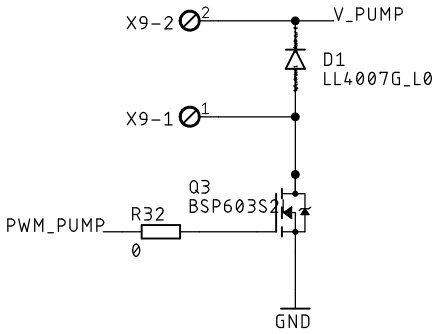

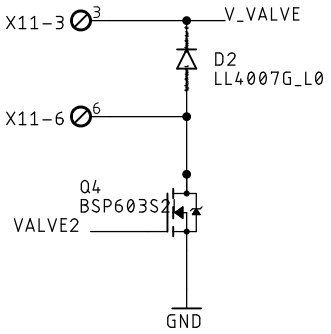

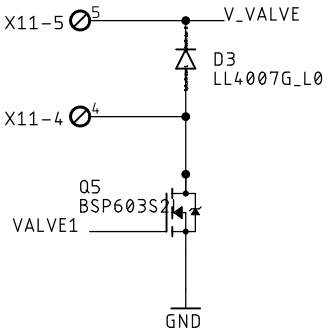

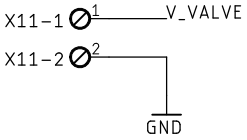

TITLE: csb		
Document Number:		REV:
Date: 25.09.2019 13:44	Sheet: 8/8	

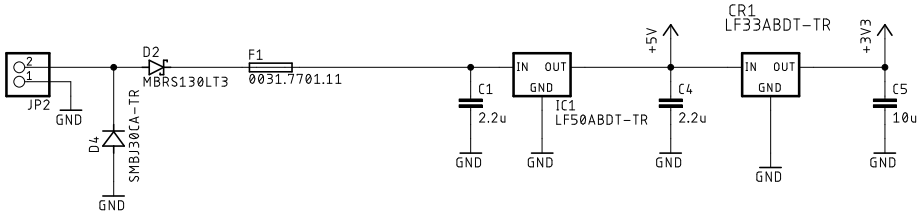

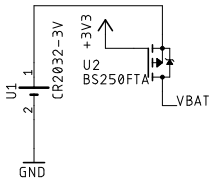

H5 MOUNT-HOLE3.0

H6 MOUNT-HOLE3.0

H7 MOUNT-HOLE3.0

H8 MOUNT-HOLE3.0

TITLE: mainboard	
Document Number:	REV:
Date: 18.10.2019 10:49	Sheet: 1/3

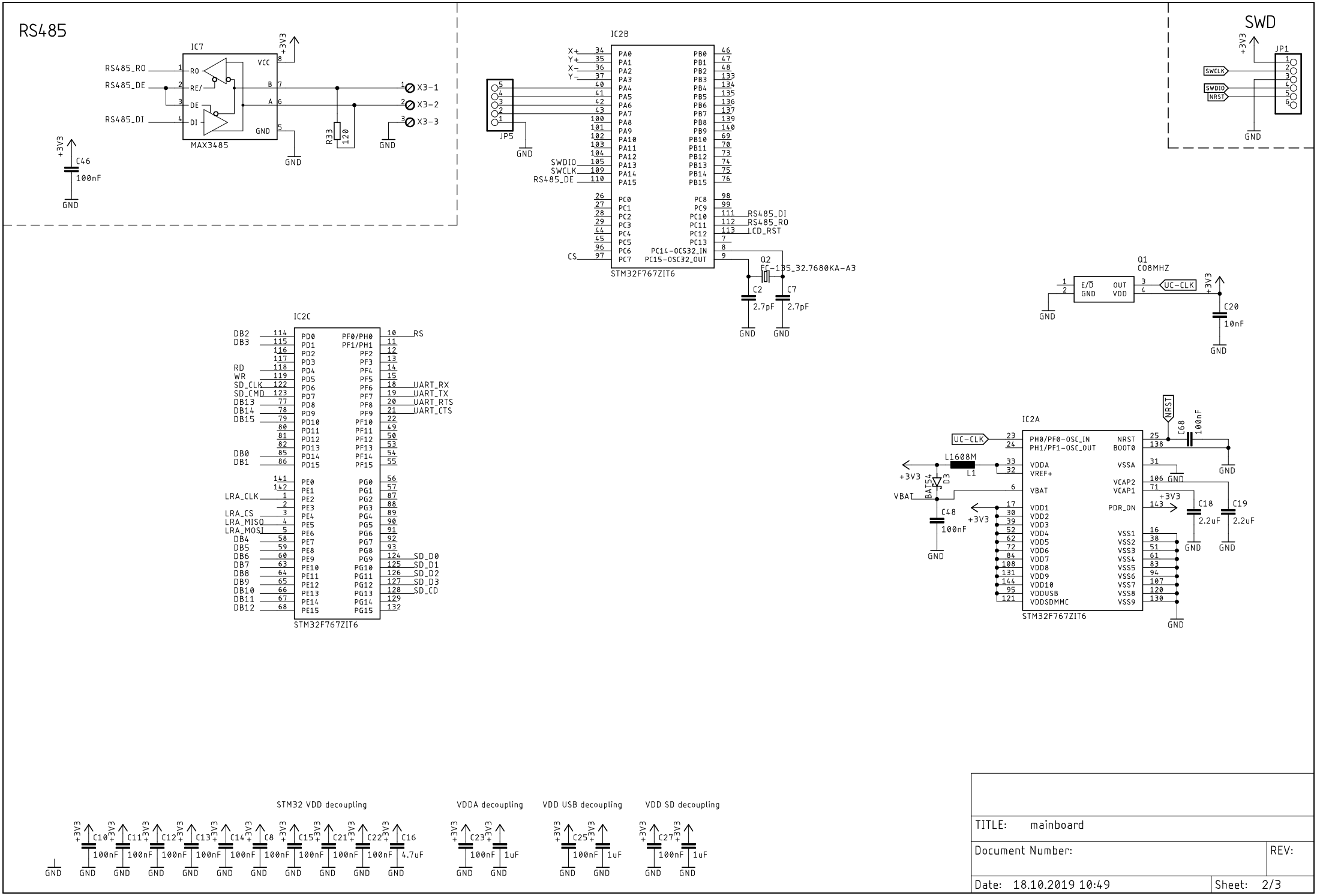
RS485
IC7
MAX3485
RS485_RO
RS485_DE
RS485_DI
RO
RE/
DE
DI
VCC
GND
B
A
+3V3
X3-1
X3-2
X3-3
R33
120
C46
100nF
IC2B
STM32F767ZIT6
JP5
SWDIO
SWCLK
RS485_DE
CS
RS485_DI
RS485_RO
LCD_RST
Q2
FC-135_32.7680KA-A3
C2
2.7pF
C7
2.7pF
SWD
JP1
SWCLK
SWDIO
NRST
Q1
C08MHZ
E/D
OUT
VDD
UC-CLK
C20
10nF
IC2C
STM32F767ZIT6
DB2
DB3
RD
WR
SD_CLK
SD_CMD
DB13
DB14
DB15
DB0
DB1
LRA_CLK
LRA_CS
LRA_MISO
LRA_MOSI
DB4
DB5
DB6
DB7
DB8
DB9
DB10
DB11
DB12
RS
UART_RX
UART_TX
UART_RTS
UART_CTS
SD_D0
SD_D1
SD_D2
SD_D3
SD_CD
IC2A
STM32F767ZIT6
L1608M
L1
BAT54
D3
VBAT
C48
100nF
C68
100nF
NRST
BOOT0
PDR_ON
C18
2.2uF
C19
2.2uF
STM32 VDD decoupling
VDDA decoupling
VDD USB decoupling
VDD SD decoupling
C10
C11
C12
C13
C14
C8
C15
C21
C22
C16
4.7uF
C23
1uF
C25
1uF
C27
1uF
TITLE: mainboard
Document Number:
REV:
Date: 18.10.2019 10:49
Sheet: 2/3

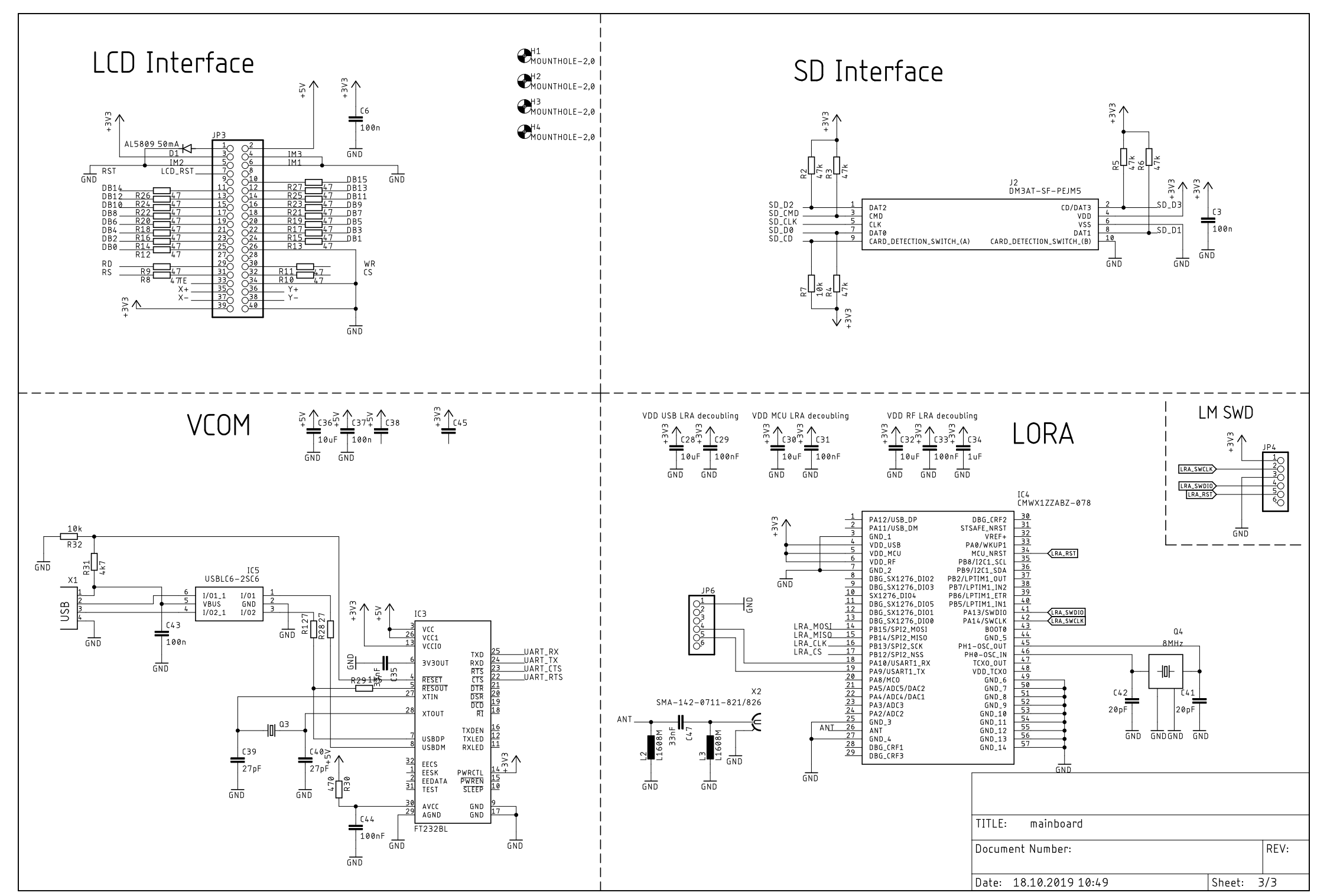
LCD Interface
SD Interface
VCOM
LORA
LM SWD
H1 MOUNTHOLE-2,0
H2 MOUNTHOLE-2,0
H3 MOUNTHOLE-2,0
H4 MOUNTHOLE-2,0
JP3
AL5809 50mA
D1
IM2
IM3
IM1
LCD_RST
RST
RD
RS
WR
CS
X+
X-
Y+
Y-
DB15
DB14
DB13
DB12
DB11
DB10
DB9
DB8
DB7
DB6
DB5
DB4
DB3
DB2
DB1
DB0
J2
DM3AT-SF-PEJM5
SD_D2
SD_CMD
SD_CLK
SD_D0
SD_CD
SD_D3
SD_D1
DAT2
CMD
CLK
DAT0
CARD_DETECTION_SWITCH_(A)
CD/DAT3
VDD
VSS
DAT1
CARD_DETECTION_SWITCH_(B)
VDD USB LRA decoubling
VDD MCU LRA decoubling
VDD RF LRA decoubling
IC4
CMWX1ZZABZ-078
PA12/USB_DP
PA11/USB_DM
VDD_USB
VDD_MCU
VDD_RF
DBG_SX1276_DIO2
DBG_SX1276_DIO3
SX1276_DIO4
DBG_SX1276_DIO5
DBG_SX1276_DIO1
DBG_SX1276_DIO0
PB15/SPI2_MOSI
PB14/SPI2_MISO
PB13/SPI2_SCK
PB12/SPI2_NSS
PA10/USART1_RX
PA9/USART1_TX
PA8/MCO
PA5/ADC5/DAC2
PA4/ADC4/DAC1
PA3/ADC3
PA2/ADC2
GND_3
ANT
GND_4
DBG_CRF1
DBG_CRF3
DBG_CRF2
STSAFE_NRST
VREF+
PA0/WKUP1
MCU_NRST
PB8/I2C1_SCL
PB9/I2C1_SDA
PB2/LPTIM1_OUT
PB7/LPTIM1_IN2
PB6/LPTIM1_ETR
PB5/LPTIM1_IN1
PA13/SWDIO
PA14/SWCLK
BOOT0
GND_5
PH1-OSC_OUT
PH0-OSC_IN
TCXO_OUT
VDD_TCXO
GND_6
GND_7
GND_8
GND_9
GND_10
GND_11
GND_12
GND_13
GND_14
LRA_RST
LRA_SWDIO
LRA_SWCLK
LRA_MOSI
LRA_MISO
LRA_CLK
LRA_CS
JP6
X2
SMA-142-0711-821/826
Q4
8MHz
JP4
IC5
USBLC6-2SC6
IC3
FT232BL
Q3
UART_RX
UART_TX
UART_CTS
UART_RTS
USB
TITLE: mainboard
Document Number:
REV:
Date: 18.10.2019 10:49
Sheet: 3/3